2023-09

Instability of waves in deep water A discrete Hamiltonian approach

Andrade, D

10.1016/j.euromechflu.2023.06.008
European Journal of Mechanics - B/Fluids
Elsevier BV

European Journal of Mechanics / B Fluids 101 (2023) 320–336

Contents lists available at ScienceDirect

European Journal of Mechanics / B Fluids

journal homepage: www.elsevier.com/locate/ejmflu

Instability of waves in deep water — A discrete Hamiltonian approach

David Andrade [a,b], Raphael Stuhlmeier [a,*]

[a] Centre for Mathematical Sciences, University of Plymouth, Plymouth, PL4 8AA, United Kingdom
[b] School of Engineering, Science and Technology, Universidad del Rosario, Bogota, 111711, Colombia

ARTICLE INFO

Article history:
Received 10 February 2023
Received in revised form 26 June 2023
Accepted 28 June 2023
Available online 4 July 2023

Keywords:
Water waves
Wave–wave interaction
Weakly-nonlinear surface waves
Instability
Hamiltonian systems

ABSTRACT

The stability of waves in deep water has classically been approached via linear stability analysis, with various model equations, such as the nonlinear Schrödinger equation, serving as points of departure. Some of the most well-studied instabilities involve the interaction of four waves – so called Type I instabilities – or five waves – Type II instabilities. A unified description of four and five wave interaction can be provided by the reduced Hamiltonian derived by Krasitskii (1994). Exploiting additional conservation laws, the discretised Hamiltonian may be used to shed light on these four and five wave instabilities without restrictions on spectral bandwidth. We derive equivalent autonomous, planar dynamical systems which allow for straightforward insight into the emergence of instability and the long time dynamics. They also yield new steady-state solutions, as well as discrete breathers associated with heteroclinic orbits in the phase space.

1. Introduction

For weakly nonlinear waves on the surface of deep water, interaction plays a role when the nonlinearity is cubic or higher. This consequence of the dispersion relation was initially investigated by Phillips [1], Longuet-Higgins [2], and Benney [3], and its ramifications on wave propagation are still being explored to this day, in stochastic wave forecasts [4], interaction of random waves with structures [5,6], phase-resolved forecasting [7,8], and numerous other threads of theoretical and applied research. At second order in the wave steepness ϵ waves do not interact to exchange energy. At third order, combinations of wavenumber vectors satisfying $\mathbf{k}_a + \mathbf{k}_b = \mathbf{k}_c + \mathbf{k}_d$ can be found to exchange energy. At fourth order this extends to $\mathbf{k}_a + \mathbf{k}_b = \mathbf{k}_c + \mathbf{k}_d + \mathbf{k}_e$. Various well-known instabilities of water waves arise as a consequence of these resonance conditions.

In the usual mathematical sense, instability requires that we start from a solution to a set of equations, and describes the evolution of disturbances of that solution. The handful of explicit solutions – to third and fourth order in nonlinearity – therefore form the backbone of classical instability results. These are the monochromatic wave which solves the problem at third order (associated with Benjamin-Feir and Type Ib instability) and fourth order (associated with Type II instability), as well as the bichromatic wave train at third order (associated with Type Ia instability, see below).

The instabilities which we will address have been approached through a combination of analytical, numerical, and experimental work (see the engaging historical review by Zakharov & Ostrovsky [9] and e.g. Mei et al. [10, Ch. 13–14] for references and an exposition focused on the Zakharov equation and the nonlinear Schrödinger equation (NLS)). The existence of different approaches, techniques, and model equations makes a simple classification of instability results difficult. Mathematically, we may identify whether the fundamental interaction is of third or fourth order in nonlinearity. Experimentally, it is often easier to classify an instability based on whether the unstable perturbations are unidirectional or multidirectional, and what wave steepness enables their growth.

We shall investigate two principal classes of instability: those involving four waves (called Type I) and those involving five waves (called Type II). Type I encompasses initial states which are plane waves or bichromatic states, and perturbations which are unidirectional or bidirectional. The Benjamin-Feir instability, which arises from a single Stokes' wave and whose most unstable perturbation is unidirectional, is the best known Type I instability. However, with four waves satisfying $\mathbf{k}_1 + \mathbf{k}_2 = \mathbf{k}_3 + \mathbf{k}_4$ there is also the possibility that two modes $\mathbf{k}_1$, $\mathbf{k}_2$ form a bichromatic wave train which is perturbed by a small bichromatic disturbance $\mathbf{k}_3$, $\mathbf{k}_4$, termed Type Ia after Ioualalen & Kharif [11]. Such cases have been studied by Dias & Hărăguş-Courcelle [12] using a dynamical systems approach in the framework of Benney–Roskes–Davey–Stewartson equations, generalising similar results for NLS. They have been investigated numerically by Fructus et al. [13] and Kimmoun et al. [14], and experimentally by Hammack et al. [15], who compared their results with solutions to

* Corresponding author.
E-mail address: raphael.stuhlmeier@plymouth.ac.uk (R. Stuhlmeier).

https://doi.org/10.1016/j.euromechflu.2023.06.008

the NLS. They also include cases of standing waves, such as those investigated by Okamura [16], who derived a set of coupled NLS equations using the Zakharov equation approach.

McLean [17] was the first to observe, via a numerical treatment, that the dominant instability changes from a two-dimensional perturbation to a three-dimensional one as the wave steepness increases. This provided a possible theoretical mechanism for the experimental work of Su [18] on crescent wave patterns, and opened up the investigation of so-called Type II instabilities, which are associated with quintet interactions. A clear exposition of this is given by Stiassnie & Shemer [19], who considered McLean's Type II results from the perspective of the Zakharov equation. Numerous numerical investigations followed, including Ioualalen & Kharif [11], who called this Type IIb, Fructus et al. [13], Fuhrman et al. [20] (using a high-order Boussinesq model), Kimmoun et al. [14], and others. We follow Ioualalen & Kharif [11] in denoting McLean's quintet instability of a Stokes' wave as Type IIb. A key theoretical advance on crescent wave patterns was made by Shrira et al. [21], who used the idea of reducing Type II instability with damping to a planar dynamical system to provide an analytical foundation for their appearance. Theoretical advances continued to go hand-in-hand with experiments, as in the work of Collard & Caulliez [22] who reported on the selection of particular harmonics in a flume experiment. Seeking to prevent wave breaking and thereby to isolate the instability leading to crescent patterns, they covered the flume surface with a thin plastic film. Fuhrman & Madsen [23] subsequently explained this selection in terms of the finite tank width used in the experiments. Interest in Type II instabilities continues unabated to the present day [24].

In the present article, we will show that the classical instabilities of deep water waves can be fully described in the elementary framework of planar dynamical systems. Our classification is based on the resonance condition on the interacting wavenumbers as follows:

1. (Type Ia) $\mathbf{k}_1+\mathbf{k}_2 = \mathbf{k}_3+\mathbf{k}_4$ – the instability of a bichromatic sea to bichromatic disturbances.
2. (Type Ib) $2\mathbf{k}_1 = \mathbf{k}_3 + \mathbf{k}_4$, with $\mathbf{k}_2$ noninteracting – the cubically nonlinear instability of a Stokes' wave to side-band disturbances (with or without a non-interacting satellite).
3. (Type IIb) $3\mathbf{k}_1 = \mathbf{k}_2 + \mathbf{k}_3$ – the quartically nonlinear instability of a Stokes' wave to side-band disturbances.

The Type Ib instability contains as a special case the Benjamin-Feir instability, which is realised when the non-interacting wave $\mathbf{k}_2$ has no energy, and only the degenerate quartet $2\mathbf{k}_1 = \mathbf{k}_3+\mathbf{k}_4$ remains. Our notation follows that of Ioualalen & Kharif [11] and Leblanc [25], who investigated Type Ia and Ib instabilities via linear stability analysis of the discrete Zakharov equation (see also Badulin et al. [26]), and Stiassnie & Shemer [19] who did the same for the Type IIb instability. The techniques we employ consist of reducing each resonantly interacting set to a planar system, in which a single phase (called the dynamic phase) and a single amplitude parameter are seen to govern the dynamics. This extends and provides a more systematic approach than previous work on the Benjamin-Feir instability [27]. Similar techniques have been employed on three-mode discretisations of the NLS [28], on the Type II instability [21], and on a system of interacting Benjamin-Feir resonances [29].

In what follows, we will describe each of these instabilities based on its corresponding discretised Hamiltonian. The Hamiltonian description which forms our starting point has no restriction on spectral bandwidth, and so contrasts with approaches based on NLS-type equations. We begin with the four-wave interactions in Section 2, where we initially treat Type Ia instability in Sections 2.1–2.2, and subsequently Type Ib in Sections 2.3–2.4. Section 3 is devoted to the study of Type II instability. Section 4 provides a discussion of our results and prospects for future work. Finally, three Appendices A, B and C provide formulas for certain coefficients, details of the asymmetric Type Ia instability, and further details about a new Type II case, respectively.

2. The discrete Hamiltonian formulation for four-wave interactions

The Hamiltonian formulation of the water wave problem was first given by Zakharov [30], and has been extensively used since then in theoretical and applied studies. Of particular practical importance is the so-called reduced equation, written in terms of an auxiliary complex variable which is related to the physical variables ζ and ϕ^s – the surface elevation and potential at the free surface, respectively – via Fourier transforms (see [10, (14.2.13)]). The definitive formulation of these reduced equations up to and including terms of fourth order in nonlinearity (quintet interactions) was given by Krasitskii [31].

We begin with the reduced Hamiltonian of the water wave problem in the discrete formulation, and up to third order in nonlinearity, cf. [31, Eq. (2.22)]:

$$H(b_1 \dots b_N, b_1^* \dots b_N^*) = \sum_{i=1}^{N} \omega_i |b_i|^2 + \frac{1}{2} \sum_{i,j,k,l=1}^{N} T_{ijkl} \delta_{ij}^{kl} b_i^* b_j^* b_k b_l. \quad (1)$$

To avoid an overly bulky expression we use subscripts to denote the dependence on wavenumber, i.e. $b(\mathbf{k}_j, t) = b_j$. The * denotes the complex conjugate. The linear dispersion relation for deep water waves is $\omega_i = \sqrt{g\|\mathbf{k}_i\|}$, with g the gravitational acceleration. Note that $g = 1$ is used in all calculations. The Kronecker delta function is written $\delta_{ij}^{kl} = \delta(\mathbf{k}_i + \mathbf{k}_j - \mathbf{k}_k - \mathbf{k}_l)$, while the expression for the kernel $T_{ijkl} = T(\mathbf{k}_i, \mathbf{k}_j, \mathbf{k}_k, \mathbf{k}_l)$ can be found in [10,31].

The discrete Zakharov equation is obtained directly from this Hamiltonian as

$$i\frac{db_i}{dt} = \frac{\partial H}{\partial b_i^*} = \omega_i b_i + \sum_{j,k,l=1}^{N} T_{ijkl} \delta_{ij}^{kl} b_j^* b_k b_l, \quad \text{for } i = 1, \dots, N. \quad (2)$$

In fact, a similar discrete system was first obtained by Benney [3] using perturbation theory rather than the Hamiltonian formulation. It is convenient to rewrite the Hamiltonian in amplitude and phase variables which are related to the original complex amplitudes as

$$b_i = |b_i| e^{-i\phi_i}, \quad \text{for } i = 1, \dots, N. \quad (3)$$

In order to preserve the Hamiltonian structure, the functional dependence must be on $|b_i|^2$ instead of the more natural $|b_i|$. The new Hamiltonian is

$$\begin{aligned} &H(|b_1|^2, \dots, |b_N|^2, \phi_1, \dots, \phi_N) \\ &= \sum_{i=1}^{N} \omega_i |b_i|^2 + \frac{1}{2} \sum_{i,j=1}^{N} e_{ij} T_{ij} |b_i|^2 |b_j|^2 \\ &+ \frac{1}{2} \sum_{i,j=1}^{N} \sum_{k\neq i,j} \sum_{l\neq i,j} T_{ijkl} \sqrt{|b_i|^2 |b_j|^2 |b_k|^2 |b_l|^2} \delta_{ij}^{kl} \\ &\times \cos(\phi_i + \phi_j - \phi_k - \phi_l), \end{aligned} \quad (4)$$

where $e_{ij} = 1$ if $i = j$ and 2 otherwise, and we abbreviate T_{ijij} by T_{ij}. We also define the Stokes' frequency correction of the wave $\mathbf{k}_i$, given by

$$\Gamma_i = T_{ii} |b_i|^2 + 2 \sum_{j\neq i} T_{ij} |b_j|^2. \quad (5)$$

This simplification of the Hamiltonian (4) from (1) makes use of a number of symmetries of the kernel T_{ijkl}, which enforce, among other things, that the Hamiltonian is always real. The reformulation already lays bare the dependence on the phases: for each nontrivial resonant interaction between four modes $\mathbf{k}_i + \mathbf{k}_j = \mathbf{k}_k + \mathbf{k}_l$ there is a single dynamic phase $\phi_i + \phi_j - \phi_k - \phi_l$. This important fact will be exploited in what follows.

Finally, the Zakharov equation written in terms of the amplitudes and phases is obtained from Hamilton's equations

$$\begin{aligned} \frac{d|b_i|^2}{dt} &= -\frac{\partial H}{\partial \phi_i}, \\ \frac{d\phi_i}{dt} &= \frac{\partial H}{\partial |b_i|^2}, \end{aligned} \qquad \text{for } i = 1\ldots, N. \tag{6}$$

Once the Zakharov equation is solved one can define the complex amplitude as

$$\mathcal{A}(\mathbf{x}, t) = \frac{1}{\pi}\sum_{j=1}^{N}\sqrt{\frac{\omega_j}{2g}}b_j e^{i(\mathbf{k}_j\cdot\mathbf{x}-\omega_j t)}, \tag{7}$$

of which the real part is the free surface elevation and the modulus is its envelope.

2.1. Hamiltonian formulation of Type Ia instability

In Type Ia instability the resonant interaction is between four distinct waves satisfying $\mathbf{k}_1 + \mathbf{k}_2 = \mathbf{k}_3 + \mathbf{k}_4$. The discrete Hamiltonian (4) becomes

$$\begin{aligned} H = &\sum_{i=1}^{4}\omega_i|b_i|^2 + \frac{1}{2}\sum_{i,j=1}^{4}e_{ij}T_{ij}|b_i|^2|b_j|^2 \\ &+ 4T_{1234}\sqrt{|b_1|^2|b_2|^2|b_3|^2|b_4|^2}\cos(\phi_1+\phi_2-\phi_3-\phi_4), \end{aligned} \tag{8}$$

and the corresponding equations of motion are

$$\begin{aligned} \frac{d|b_{1,2}|^2}{dt} &= -\frac{\partial H}{\partial \phi_{1,2}} \\ &= 4T_{1234}\sqrt{|b_1|^2|b_2|^2|b_3|^2|b_4|^2}\sin(\phi_1+\phi_2-\phi_3-\phi_4), \end{aligned} \tag{9}$$

$$\begin{aligned} \frac{d|b_{3,4}|^2}{dt} &= -\frac{\partial H}{\partial \phi_{3,4}} \\ &= -4T_{1234}\sqrt{|b_1|^2|b_2|^2|b_3|^2|b_4|^2}\sin(\phi_1+\phi_2-\phi_3-\phi_4), \end{aligned} \tag{10}$$

$$\begin{aligned} \frac{d\phi_i}{dt} &= \frac{\partial H}{\partial |b_i|^2} \\ &= \omega_i + \Gamma_i + 2T_{1234}\frac{\sqrt{|b_1|^2|b_2|^2|b_3|^2|b_4|^2}}{|b_i|^2} \\ &\quad\times \cos(\phi_1+\phi_2-\phi_3-\phi_4), \quad \text{for } i = 1, 2, 3, 4. \end{aligned} \tag{11}$$

The equations of motion form a system of eight coupled ODEs for the amplitudes and phases. As noted above, the phases appear only in the combination $\theta = \phi_1 + \phi_2 - \phi_3 - \phi_4$, the dynamic phase of the Type Ia problem. This fact was already pointed out by Bretherton [32] in the case of an interacting triad, and has been used extensively in studies of discrete wave–wave interaction (see Stiassnie & Shemer [33], Craik [34]).[1] In fact, exploiting the other invariants of the cubic Zakharov equation we will reduce the eight ODEs to a planar system involving a single amplitude and the dynamic phase.

In addition to the Hamiltonian, the momentum $\mathbf{M}$ and total wave action A

$$\mathbf{M} = \sum_{i=1}^{4}\mathbf{k}_i|b_i|^2, \qquad A = \sum_{i=1}^{4}|b_i|^2, \tag{12}$$

are conserved (see [31, Eq. (3.36)ff]). We can write these conservation laws, denoting $\mathbf{M} = (M^x, M^y)$ and $\mathbf{k}_i = (k_i, l_i)$ in matrix form as

$$K\mathbf{b} = \begin{pmatrix} 1 & 1 & 1 & 1 \\ k_1 & k_2 & k_3 & k_4 \\ l_1 & l_2 & l_3 & l_4 \end{pmatrix}\begin{pmatrix} |b_1(t)|^2 \\ |b_2(t)|^2 \\ |b_3(t)|^2 \\ |b_4(t)|^2 \end{pmatrix} = \begin{pmatrix} A \\ M^x \\ M^y \end{pmatrix}. \tag{13}$$

Thus far no mention of instability has been made: indeed, the system of Eqs. (9)–(11) contains many possible solutions – including single mode Stokes' waves, bichromatic waves, and resonantly interacting quartets (an exact, general solution can be written in terms of Jacobian elliptic functions, see [33]) – constrained in wave action and momentum by (13).

Type Ia instability arises from one of these solutions: the well-known bichromatic solution to the Zakharov equation [10, Ch. 14.6] consisting of modes $\mathbf{k}_1, \mathbf{k}_2$. In fact, this is precisely the case first described by Longuet-Higgins and Phillips [36], where each wave train effects a correction to the frequency of the other, but no energy exchange takes place.

If we start with a bichromatic wave-train consisting of wavenumbers $\mathbf{k}_1$ and $\mathbf{k}_2$, the momentum is the vector $\mathbf{M} = \mathbf{k}_1|b_1(0)|^2 + \mathbf{k}_2|b_2(0)|^2$, while the wave action is simply $A = |b_1(0)|^2 + |b_2(0)|^2$. This configuration corresponds to the particular solution $\mathbf{b} = (|b_1(0)|^2, |b_2(0)|^2, 0, 0)$ of (13). Now we know that the right-hand side of system (13) is constant, as is the coefficient matrix K. This coefficient matrix is of rank 3, and its null space is spanned by $(1, 1, -1, -1)$, as a consequence of the Type Ia resonance condition. This leads us to the following (time-dependent) general solution to the quartet-interaction problem when starting from a bichromatic sea: $\mathbf{b} = (|b_1(0)|^2 - f(t), |b_2(0)|^2 - f(t), f(t), f(t))$, for some smooth function $f(t)$ with $f(0) = 0$.

The flow of energy is thus constrained: an initially bichromatic wave train may only transfer energy symmetrically to a resonantly interacting bichromatic wave train – the classical instability setting. Restricting ourselves to symmetric initial conditions $|b_1(0)|^2 = |b_2(0)|^2$ we can then write the amplitudes in terms of a parameter η (ranging between 0 and 1/2) as

$$|b_1|^2 = A\eta, \tag{14a}$$

$$|b_2|^2 = A\eta, \tag{14b}$$

$$|b_3|^2 = A(1/2 - \eta), \tag{14c}$$

$$|b_4|^2 = A(1/2 - \eta). \tag{14d}$$

From a geometrical point of view this solution (14) corresponds to $\mathbf{M}/A = (\mathbf{k}_1+\mathbf{k}_2)/2 = (\mathbf{k}_3+\mathbf{k}_4)/2$ as shown in Fig. 1 (left panel). Physically the parameter η governs how the total wave action is partitioned among the modes, under the assumption that there is initially an equidistribution among modes $\mathbf{k}_1$ and $\mathbf{k}_2$; this enforces equidistribution among $\mathbf{k}_3$ and $\mathbf{k}_4$, as shown above. Other initial states can be selected, however this is the only choice which supports total energy transfer between two bichromatic sea-states (see Appendix B).

The amplitude parameter η now takes the role of a new variable for the problem

$$\frac{d\eta}{dt} = \frac{1}{A}\frac{d|b_1|^2}{dt} = -\frac{\partial H}{\partial \phi_1} = 2AT_{1234}\eta(1-2\eta)\sin(\theta), \tag{15}$$

[1] Note that the sign convention (3) is opposite to that used in [27,35], which leads to the appearance of a factor of −1 in the equations.

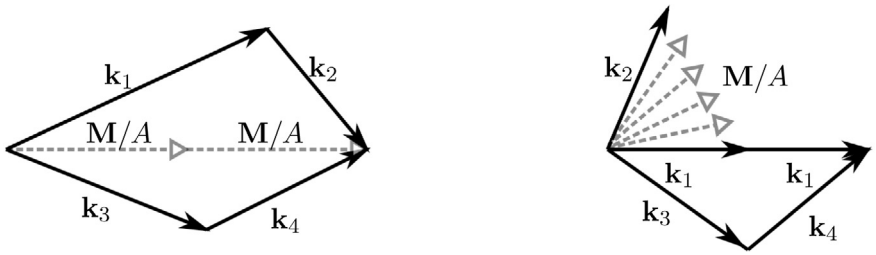

Fig. 1. Relationship between resonant wavenumber vectors and normalised momentum $\mathbf{M}/A$ in Type Ia (left) and Type Ib (right).

where $\theta = \phi_1+\phi_2-\phi_3-\phi_4$ is the dynamic phase. In fact, the pair η and θ can be seen as conjugate variables for a new Hamiltonian $\tilde{H}$

$$\tilde{H}(\eta,\theta) = -2AT_{1234}\eta(1-2\eta)\cos(\theta)-(\Delta_{12}^{34}+A\Omega_0)\eta-\frac{A\Omega_1}{2}\eta^2, \quad (16)$$

where the coefficients are found by writing the Stokes' corrections as a degree one polynomial in η as

$$\Gamma_1+\Gamma_2-\Gamma_3-\Gamma_4 = A\Omega_0+A\Omega_1\eta. \quad (17)$$

Here Δ_{12}^{34} denotes the frequency detuning $\omega_1+\omega_2-\omega_3-\omega_4$, and the full expressions for Ω_0 and Ω_1 can be found in Appendix A.

2.2. Dynamics of Type Ia

In terms of the new variables, the system of ODEs governing Type Ia instability is given by

$$\frac{d\eta}{dt} = \frac{\partial\tilde{H}}{\partial\theta} = 2AT_{1234}\eta(1-2\eta)\sin(\theta), \quad (18)$$

$$\frac{d\theta}{dt} = -\frac{\partial\tilde{H}}{\partial\eta} = \Delta_{12}^{34}+A\Omega_0+A\Omega_1\eta+2AT_{1234}(1-4\eta)\cos(\theta), \quad (19)$$

derived from the new Hamiltonian (16).

Recall that $\eta \in [0, 1/2]$, and the dynamic phase $\theta \in [-\pi, \pi)$ – this means the phase plane is the surface of a truncated cylinder of height 1/2. The top and bottom of the cylinder correspond to bichromatic wave trains: at the base of the cylinder $\eta = 0$ the wave action is equally distributed in the modes $\mathbf{k}_3$ and $\mathbf{k}_4$, with no energy in the modes $\mathbf{k}_1$ and $\mathbf{k}_2$. At $\eta = 1/2$ the situation reverses. Any point in the interior of the phase-plane represents a quartet of water waves, describing the interactions of the two bichromatic wave trains.

For a physically meaningful treatment, we relate the magnitude of the complex amplitudes to the physical amplitudes a_i of Stokes' waves (see [10, Sec. 14.6]) via

$$|b_1| = 2\pi\sqrt{\frac{g}{2\omega_1}}a_1, \quad |b_2| = 2\pi\sqrt{\frac{g}{2\omega_2}}a_2. \quad (20)$$

We also relate the total wave action A to the steepness $\epsilon_i = a_i|k_i|$ of the initial bichromatic sea-state, consisting of two constant amplitudes Stokes' waves, as

$$A = 2\pi^2\left(\frac{\omega_1}{k_1^3}\epsilon_1^2+\frac{\omega_2}{k_2^3}\epsilon_2^2\right). \quad (21)$$

2.2.1. Fixed points and heteroclinic connections

As is customary when dealing with dynamical systems, we begin by looking for stationary solutions, or fixed points, of Eqs. (18)–(19). The Hamiltonian structure of the planar system means that the Jacobi matrix J has the form

$$J = \begin{pmatrix} H_{\eta\theta} & H_{\theta\theta} \\ -H_{\eta\eta} & -H_{\eta\theta} \end{pmatrix}, \quad (22)$$

vanishing trace, and determinant $\det(J) = H_{\theta\theta}H_{\eta\eta}-H_{\eta\theta}^2$. This implies that the eigenvalues of the Jacobi matrix, which determine the linear stability of fixed points, satisfy $\lambda_{1,2} = \pm\sqrt{-\det(J)}$, and ensures that all fixed points which appear are either centres or saddle points. Our next task will be to find these fixed points.

In terms of their location in the phase space there are four kinds of possible fixed points, which we can classify as shown in Table 1, where we also give their corresponding values of the Hamiltonian. The four classes of fixed points can occur in essentially four generic configurations, which are depicted in Fig. 2 (a special configuration shown in panel (e) is discussed further in Section 2.2.2). In the absence of fixed points the orbits in phase space are nearly horizontal, as little energy exchange takes place (no substantial changes in η). The appearance of distinct fixed points, and the separatrices which connect them, change this behaviour, and highlight configurations in which energy exchange takes place as the orbits wind between the separatrices.

At the top ($\eta = 1/2$) and bottom ($\eta = 0$) of the phase space, where the right-hand side of Eq. (18) vanishes, the Jacobi matrix is

$$J_\pm = \begin{pmatrix} \mp 2AT_{1234}\sin(\theta) & 0 \\ -8AT_{1234}\cos(\theta)+A\Omega 1 & \pm 2AT_{1234}\sin(\theta) \end{pmatrix}, \quad (23)$$

where J_+ corresponds to $\eta = 1/2$ and J_- to $\eta = 0$. The Jacobi determinant in either case $\det(J) = -4A^2T_{1234}^2\sin(\theta)^2 \le 0$. This expression vanishes when $\theta = 0, \pm\pi$, but in all other cases fixed points occurring there must be saddle points. Those fixed points must solve (19) with $d\theta/dt = 0$, which condition yields the values found in Table 1.

We consider the fixed points at $\eta = 1/2$: these have Jacobi determinant

$$\det(J) = \left(\Delta_{12}^{34}+\Gamma_1+\Gamma_2-\Gamma_3-\Gamma_4\right)-16|b_1|^2|b_2|^2T_{1234}^2, \quad (24)$$

where we have used the fact that $|b_3| = |b_4| = 0$ on $\eta = 1/2$ and $|b_1|^2 = |b_2|^2 = A/2$ to simplify the expression. In fact, the condition of real eigenvalues, $\det(J) \le 0$, is precisely the condition for existence of these fixed points, as can be seen by squaring the value of $\cos(\theta)$ given in Table 1. We recognise that the condition $\det(J) < 0$ for the existence of distinct saddle points at $\eta = 1/2$ is identical to the linear stability condition found by [25, Eq. 15] (note that the use of Δ and Γ therein differs from the present manuscript). These fixed points appear from a zero-eigenvalue bifurcation which occurs at either $\theta = 0$ (cf. the setting in panel (b) of Fig. 2) or at $\theta = \pm\pi$ (cf. the setting in panel (a) of Fig. 2). Symmetry of our system means these fixed points appear symmetric about $\theta = 0$. It is worth noting that our analysis has assumed initially equal magnitudes $|b_1(0)| = |b_2(0)|$, in contrast to the linear stability analysis of Leblanc [25]; the above results on the instability of a bichromatic wave train can easily be carried out for $\alpha := (|b_1(0)|^2-|b_2(0)|^2)/A \neq 0$, (see Appendix B) but the reader should note that this changes the phase portraits away from the initial configuration.

It is possible to show directly the existence of heteroclinic orbits connecting the saddle points. When distinct, nonzero eigenvalues exist, i.e. in those settings with two fixed points and

Table 1
Fixed points for the Type Ia instability (18)–(19). Each row depicts a fixed point, with corresponding value of amplitude parameter η, dynamic phase θ, and value of the Hamiltonian $\tilde{H}$.

η	θ	$\tilde{H}$
0	$\pm\arccos\left(-\frac{A\Omega_0+\Delta_{12}^{34}}{2AT_{1234}}\right)$	0
1/2	$\pm\arccos\left(\frac{2A\Omega_0+A\Omega_1+2\Delta_{12}^{34}}{4AT_{1234}}\right)$	$-\frac{4(\Delta_{12}^{34}+A\Omega_0)+A\Omega_1}{8}$
$-\frac{A\Omega_0-2AT_{1234}+\Delta_{12}^{34}}{A(\Omega_1+8T_{1234})}$	$\pm\pi$	$\frac{\left(2AT_{1234}-A\Omega_0-\Delta_{12}^{34}\right)^2}{(16T_{1234}+2\Omega_1)A}$
$-\frac{A\Omega_0+2AT_{1234}+\Delta_{12}^{34}}{A(\Omega_1-8T_{1234})}$	0	$-\frac{\left(2AT_{1234}+A\Omega_0+\Delta_{12}^{34}\right)^2}{(16T_{1234}-2\Omega_1)A}$

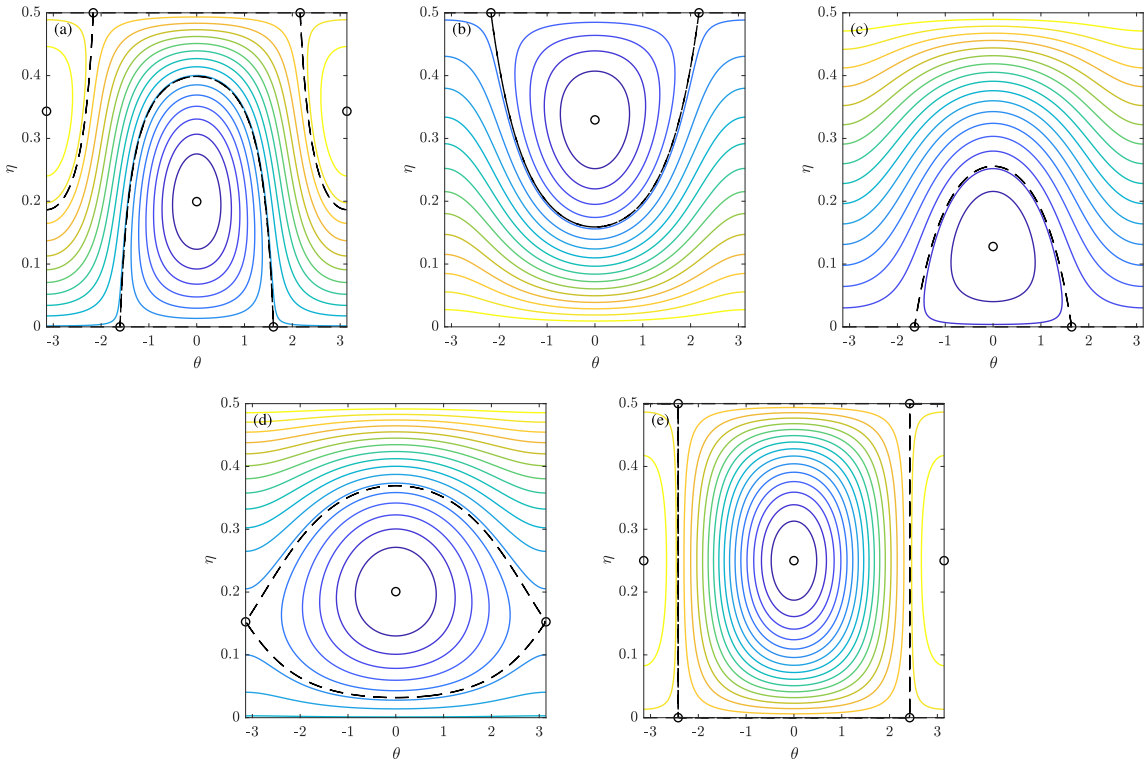

Fig. 2. Phase portraits depicting the four different configurations of fixed points which occur in the Class Ia dynamics of two bichromatic wave trains. Labels (a)–(d) correspond to labels in Fig. 3. Label (e) corresponds to the special multi-breather discussed in Section 2.2.2. In cases (a), (b) and (e) the nullcline $\eta = 1/2$ is orbitally unstable. The total wave action A corresponds to $\epsilon = 0.1$ in (21).

$\det(J) \neq 0$, these are $\lambda_{1,2} = \pm 2AT_{1234}\sin(\theta)$. Let (η^*, θ^*) be a fixed point on either boundary. It is easy to see from (23) that the eigendirections are $(\eta, \theta) = (0, 1)$ and $(1, \alpha)$. Depending on the sign of $2AT_{1234}\sin(\theta)$ one of these will be the stable and one the unstable eigendirection. This stability is reversed in the case of the fixed point $(\eta^*, -\theta^*)$. An orbit along the eigendirection $(1, \alpha)$ into the interior of the phase space must therefore connect pairs of saddle points, forming a separatrix.

Indeed, the existence of such a separatrix, heralded by the condition $\det(J) < 0$ in (24), shows that the nullcline $\eta = 1/2$ is not orbitally stable. A trajectory starting arbitrarily near $\eta = 1/2$ necessarily deflects by a fixed amount in η as it moves around the separatrix. The same holds for the nullcline $\eta = 0$.

While a classification of the dynamics is relatively straightforward, the cumbersome algebraic expressions for the kernels T and the coefficients Ω_0, Ω_1 mean that further quantitative insight relies on the choice of configuration. Specifying the wavenumbers of the bichromatic sea-state corresponding to the top of the phase-space at $\eta = 1/2$ by

$$\mathbf{k}_1 = (1, 0), \quad \mathbf{k}_2 = (\cos(\phi), \sin(\phi)), \tag{25}$$

allows us to investigate the appearance of fixed points parametrically, in terms of an auxiliary wavenumber $\mathbf{k} = (k_x, k_y)$ which is used to construct

$$\mathbf{k}_3 = \mathbf{k}_1 + \mathbf{k}, \quad \mathbf{k}_4 = \mathbf{k}_2 - \mathbf{k}. \tag{26}$$

The existence of fixed points with varying k_x and k_y is depicted in Figs. 3 and 4, where different colours denote the four different classes of fixed points (fixed points for $\eta = 0, 1/2$ and $\theta = 0, \pm\pi$ are plotted separately for legibility). The fixed points at $\eta = 1/2$ are associated with the Class Ia instability of a bichromatic wave train investigated by [25, Fig. 5]. The fixed points at $\eta = 0$ are the complementary instability of the secondary bichromatic wave train. Meanwhile, fixed points at $\theta = 0$ and $\theta = \pm\pi$ correspond to resonant or nearly resonant steady-state quartets, akin to those found by [37] (see their Appendix B).

The overlap of the regions depicted in Figs. 3 and 4 demonstrates that these occur together in large portions of parameter space. The phase portraits shown in Fig. 2 depict four characteristic cases (a)–(d), and the special case (e) which is discussed in Section 2.2.2. Cases (a)–(d) correspond to the labels in Fig. 3. It can also be observed that the generic configuration is one of periodic

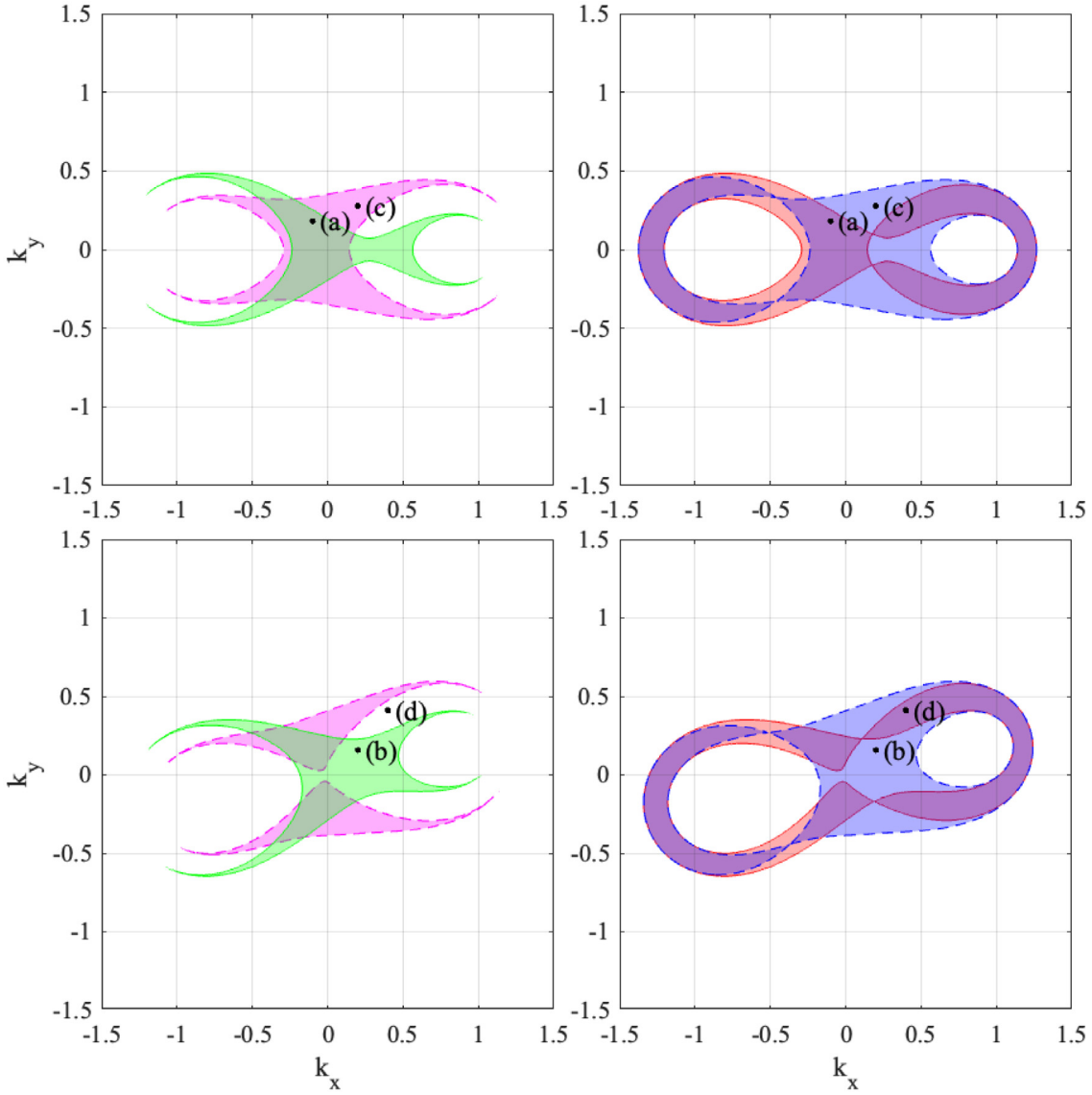

Fig. 3. Existence of fixed points in the dynamics of two bichromatic wave-trains described by (18)–(19), for various values of inclination ϕ of the primary bichromatic case: $\phi = 0$ (row 1), $\phi = \pi/8$ (row 2). The left column shows fixed points at $\eta = 1/2$ (green domain) and $\eta = 0$ (magenta domain). The right column shows fixed points at $\theta = 0$ (blue domain) and $\theta = \pm\pi$ (red domain), see Table 1. Labels (a)–(d) correspond to phase portraits plotted in Fig. 2. (For interpretation of the references to colour in this figure legend, the reader is referred to the web version of this article.)

energy exchange; however, certain trajectories are confined to a subset of the possible phase-space by the presence of a separatrix.

As the angle between the primary bichromatic waves increases the instability domain shrinks, reaching a minimum at $\phi = \pi/2$ (orthogonal primary waves), which are stable to almost all perturbations (see top panel, Fig. 4). Standing waves (see bottom panel, Fig. 4) have a characteristic symmetric instability domain – fixed points appearing when the perturbation wavenumbers lie in an annulus.

2.2.2. Type Ia multibreathers

The heteroclinic orbits shown in panels (a)–(c) of Fig. 2 connect pairs of fixed points at $\eta = 0$ and $\eta = 1/2$. These are special solutions, where a small perturbation – with the correct phase – to a bichromatic wave train gives rise to a four-wave interaction, which subsequently recedes to yield the original bichromatic wave train, albeit with a phase shift. This type of spatially periodic modulation, which arises from a bichromatic background as time $t \to \pm\infty$ corresponds to a discrete multibreather solution of the Zakharov equation. Such multibreathers are a manifestation of the underlying instability of the bichromatic wave train, and exist for many combinations of parameters (see Figs. 3–4). They can be found by integrating the equation for the orbits $d\eta/d\theta$, using the fact that the Hamiltonian along the trajectory takes the value along the boundary from which the separatrix emanates.

A special multibreather solution occurs when

$$\tilde{H}(1/2, \theta) = \tilde{H}(0, \theta). \tag{27}$$

This solution connects fixed points on the top and bottom of the phase plane, i.e. at $(\eta, \theta) = (0, \theta_0)$ and $(\eta, \theta) = (1/2, \theta_{1/2})$, as shown in panel (e) of Fig. 2. It corresponds to the complete transfer of energy from one bichromatic wave train to another, and it can be shown by direct substitution that the eigendirections of (23) are precisely (1, 0) and (0, 1).

Eq. (27) can be written as

$$A\Omega_1 + 4(A\Omega_0 + \Delta_{12}^{34}) = 0, \tag{28}$$

and this implies that the dynamic phase satisfies

$$\cos(\theta_0) = \cos(\theta_{1/2}) = \frac{\Omega_1}{8T_{1234}}. \tag{29}$$

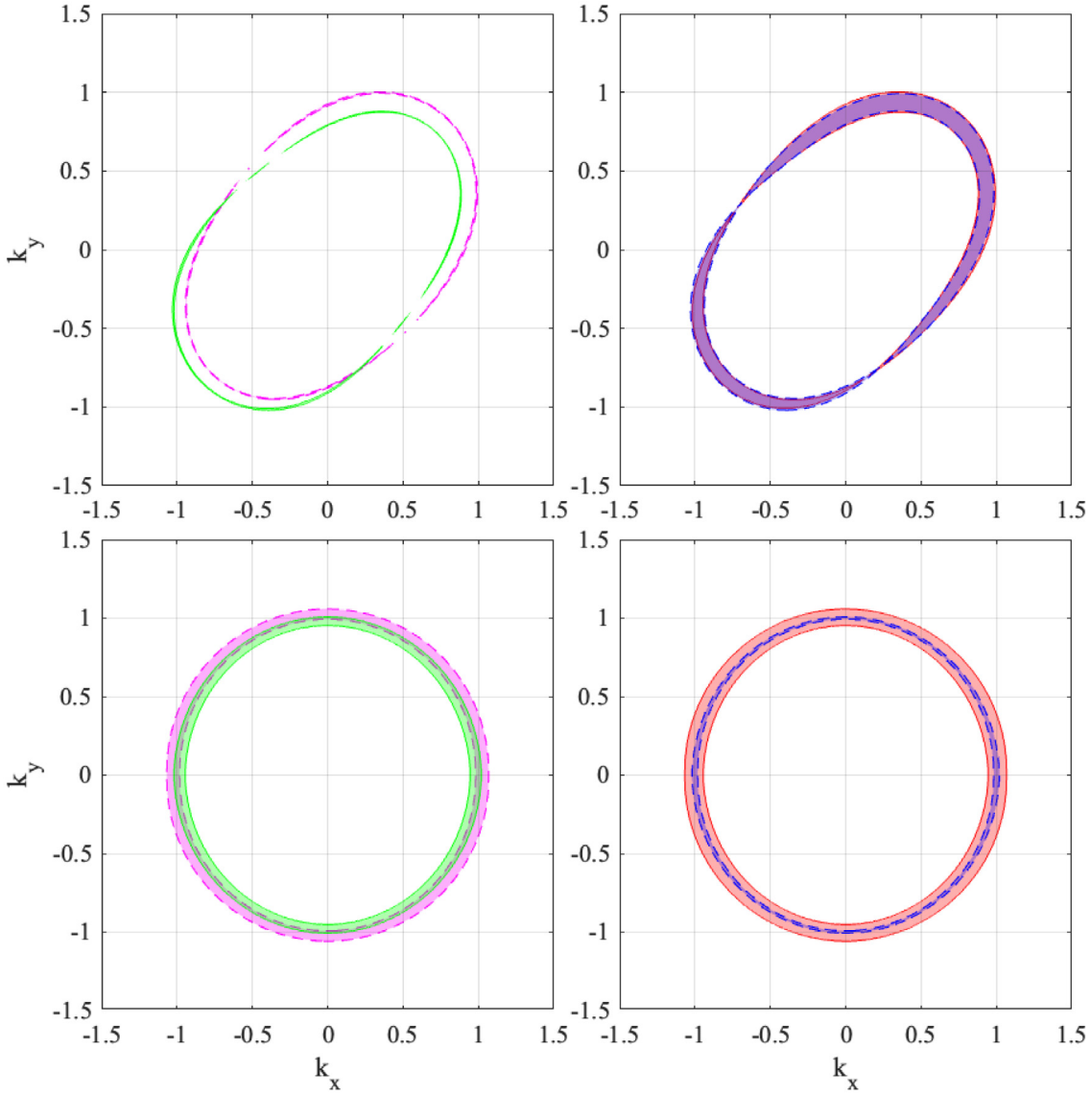

Fig. 4. Existence of fixed points in the dynamics of two bichromatic wave-trains described by (18)–(19), for various values of inclination $\phi = \pi/2$ (row 1) and $\phi = \pi$ (row 2). For description of colours see Fig. 3. (For interpretation of the references to colour in this figure legend, the reader is referred to the web version of this article.)

Thus we look for solutions with $\theta(t) = \theta_0$ which upon integration of Eq. (19) yields

$$\eta(\tilde{t}) = \frac{e^{\sin(\theta_0)\tilde{t}}}{C + 2e^{\sin(\theta_0)\tilde{t}}}, \tag{30}$$

where $C > 0$ is an integration constant and $\tilde{t} = 2AT_{1234}t$ denotes a dimensionless time scale. The choice of integration constant is arbitrary but in the following examples we shall use $C = 1$.

A second heteroclinic orbit between the fixed points $(1/2, -\theta_{1/2})$ and $(0, -\theta_0)$ can be found by replacing t with $-t$ and $\theta(t) = -\theta_0 = -\theta_1$.

While the existence of fixed points at $\eta = 0$ or $\eta = 1/2$ is enough to guarantee the existence of general multibreathers – these are simply the heteroclinic orbits connecting the fixed points – this particular case requires a careful specification of parameters. We take wave vectors $\mathbf{k}_1 = (1, 0)$, $\mathbf{k}_2 = (1, -1)$, $\mathbf{k}_3 = (1.19, -0.11)$ and $\mathbf{k}_4 = (0.80, -0.88)$ together with steepness $\epsilon_1 = 0.0843$, $\epsilon_2 = 0.13$ which yields a total wave action $A = 0.28$. The corresponding steepness of the remaining two waves are $\epsilon_3 = 0.1064$ and $\epsilon_4 = 0.1049$. This ensures the existence of fixed points at both $\eta = 1/2$ and $\eta = 0$ together with Eq. (27), and hence the existence of a heteroclinic solution linking the fixed points on the top and bottom of the phase space.

In Fig. 5 we plot the envelope of the free surface corresponding to this solution, at three instances of normalised time. This computation of (7) requires one to recover the individual phases from the amplitudes and the dynamic phase by direct numerical integration of Eq. (11). Finally the modulus of the resulting expression yields the real envelope.

Note that the envelope of the initial bichromatic sea ($\tilde{t} = 10$, bottom panel Fig. 5) is monochromatic (with wave vector $\mathbf{k} = \mathbf{k}_1 - \mathbf{k}_2 = (0, 1)$). As energy is transferred the free surface corresponds to a quartet of interacting waves, and the envelope shows a complex two-dimensional pattern ($\tilde{t} = 0$, middle panel). Finally, the energy transfer process completes and only modes $\mathbf{k}_3$ and $\mathbf{k}_4$ remain ($\tilde{t} = -10$, top panel); the envelope is again monochromatic, now with wavenumber $\mathbf{k}_3 - \mathbf{k}_4 = (0.39, 0.77)$.

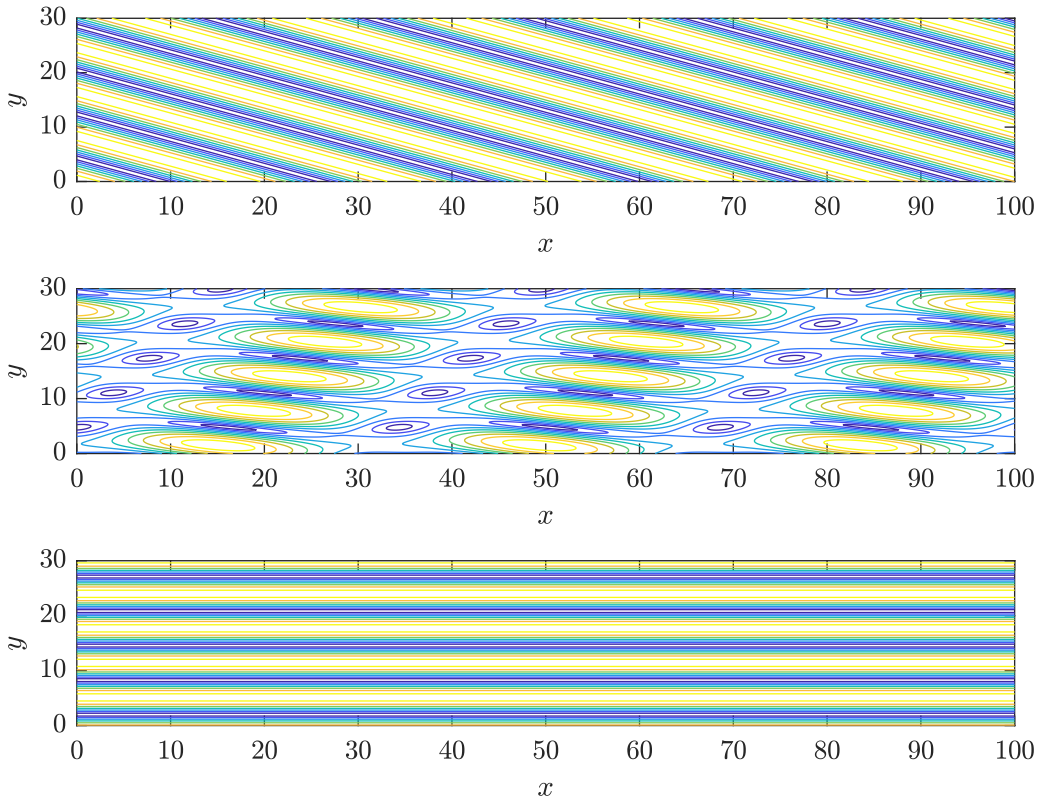

Fig. 5. Snapshots of the envelope of the free surface of a special multibreather solution. The wave components are $\mathbf{k}_1 = (1, 0)$, $\mathbf{k}_2 = (1, -1)$, $\mathbf{k}_3 = (1.19, -0.11)$ and $\mathbf{k}_4 = (0.80, -0.88)$. Total wave action is $A = 0.28$ obtained from slopes $\epsilon_1 = 0.084$, $\epsilon_2 = 0.13$. The plots are organised from top to bottom according to $\tilde{t} = -10, 0, 10$ respectively. The limiting bichromatic wave train has slopes $\epsilon_3 = 0.106$ and $\epsilon_4 = 0.104$.

2.3. Hamiltonian formulation of Type Ib instability

Type Ib instability consists of a fundamental resonance $2\mathbf{k}_1 = \mathbf{k}_3 + \mathbf{k}_4$ accompanied by a non-resonant wave $\mathbf{k}_2$. In this sense it is a generalisation of the usual Benjamin-Feir instability discussed recently by [27], which is recovered when the amplitude of mode $\mathbf{k}_2$ is set to zero. It is also prototypical for how a non-interacting wave can influence a resonant set: this influence occurs through a mutual frequency correction captured in the "Stokes' correction" terms Γ_i. The details of the analysis are similar to the Type Ia instability discussed in Sections 2.1–2.2.

With these resonance conditions, the Hamiltonian (4) becomes

$$H = \sum_{i=1}^{4} \omega_i |b_i|^2 + \frac{1}{2} \sum_{i,j=1}^{4} e_{ij} T_{ij} |b_i|^2 |b_j|^2 + 2T_{1134} |b_1|^2 \sqrt{|b_3|^2 |b_4|^2} \cos(2\phi_1 - \phi_3 - \phi_4). \tag{31}$$

Note that H does not depend on ϕ_2 so $|b_2|^2$ must be constant, i.e. mode $\mathbf{k}_2$ remains a Stokes' wave with constant amplitude. The equations of motion for the other amplitudes and phases are

$$\frac{d|b_1|^2}{dt} = -\frac{\partial H}{\partial \phi_1} = 4T_{1134} |b_1|^2 \sqrt{|b_3|^2 |b_4|^2} \sin(2\phi_1 - \phi_3 - \phi_4), \tag{32}$$

$$\frac{d|b_{3,4}|^2}{dt} = -\frac{\partial H}{\partial \phi_{3,4}} = -2T_{1134} |b_1|^2 \sqrt{|b_3|^2 |b_4|^2} \times \sin(2\phi_1 - \phi_3 - \phi_4), \tag{33}$$

$$\frac{d\phi_1}{dt} = \frac{\partial H}{\partial |b_1|^2} = \omega_1 + \Gamma_1 + 2T_{1134} \sqrt{|b_3|^2 |b_4|^2} \times \cos(2\phi_1 - \phi_3 - \phi_4), \tag{34}$$

$$\frac{d\phi_2}{dt} = \frac{\partial H}{\partial |b_2|^2} = \omega_2 + \Gamma_2, \tag{35}$$

$$\frac{d\phi_{3,4}}{dt} = \frac{\partial H}{\partial |b_{3,4}|^2} = \omega_i + \Gamma_i + T_{1134} |b_1|^2 \sqrt{\frac{|b_{4,3}|^2}{|b_{3,4}|^2}} \times \cos(2\phi_1 - \phi_3 - \phi_4), \quad i = 3,\ 4. \tag{36}$$

Note that the equations for the amplitudes and phases do not depend on ϕ_2. Hence the system decouples and the evolution of $|b_{1,3,4}|^2$ and their phases can be treated independently. Once they are solved the remaining variable, e.g. the phase ϕ_2 can be found by simple integration.

As with the Type Ia instability in Section 2.1, we reduce the degrees of freedom in the Hamiltonian to a single amplitude and a dynamic phase. Using conservation of momentum and wave action recovers a system of linear equations very similar to (13).

We rewrite the magnitudes $|b_i|^2$ of the interacting modes in terms of a new amplitude parameter η

$$|b_1|^2 = A\eta, \tag{37}$$

$$|b_3|^2 = \frac{A}{2}(D - \eta), \tag{38}$$

$$|b_4|^2 = \frac{A}{2}(D - \eta), \tag{39}$$

$$|b_2|^2 = AB, \tag{40}$$

where $D = (|b_1|^2 + |b_3|^2 + |b_4|^2)/A$ is the fraction of the total wave action in the resonant triad and $B = |b_2|^2/A$ is the fraction in the satellite wave $\mathbf{k}_2$. Conservation of wave action means $B + D = 1$. The scalar amplitude parameter η is between 0 and D, and the wave momentum is chosen so that $\mathbf{M}/A = D\mathbf{k}_1 + B\mathbf{k}_2$, i.e. the wave action is equipartitioned among the side-bands $\mathbf{k}_3$ and $\mathbf{k}_4$. The momentum can be depicted graphically as lying in the convex hull of $\mathbf{k}_1$ and $\mathbf{k}_2$, as shown in Fig. 1.

The evolution of η is governed by

$$\frac{d\eta}{dt} = \frac{1}{A}\frac{d|b_1|^2}{dt} = -\frac{1}{A}\frac{\partial H}{\partial \phi_1} = 2AT_{1134}\eta(D-\eta)\sin(\theta), \tag{41}$$

where $\theta = 2\phi_1 - \phi_3 - \phi_4$. The equation governing the dynamic phase θ is

$$\begin{aligned}\frac{d\theta}{dt} &= 2\frac{d\phi_1}{dt} - \frac{d\phi_3}{dt} - \frac{d\phi_4}{dt} = 2\frac{\partial H}{\partial |b_1|^2} - \frac{\partial H}{\partial |b_3|^2} - \frac{\partial H}{\partial |b_4|^2} \\ &= \Delta_{11}^{34} + 2\Gamma_1 - \Gamma_3 - \Gamma_4 + 2AT_{1134}(D-2\eta)\cos(\theta)\end{aligned} \tag{42}$$

where the frequency detuning is $\Delta_{11}^{34} = 2\omega_1 - \omega_3 - \omega_4$.

In this way we find that a Hamiltonian for Type Ib resonances is

$$\tilde{H}(\eta,\theta) = -\eta\left(2AT_{1134}(D-\eta)\cos(\theta) + \Delta_{11}^{34} + A\Omega_0 + \frac{A\Omega_1\eta}{2}\right). \tag{43}$$

Here the coefficients are found by writing the Stokes corrections as a degree one polynomial in the variable η as

$$2\Gamma_1 - \Gamma_3 - \Gamma_4 = A\Omega_0 + A\Omega_1\eta. \tag{44}$$

Full expressions for these coefficients can be found in Appendix A.

2.4. Dynamics of Type Ib

The dynamical system corresponding to Type Ib (a degenerate quartet and a single noninteracting satellite) is

$$\frac{d\eta}{dt} = \frac{\partial \tilde{H}}{\partial \theta} = 2\eta T_{1134}A\,(D-\eta)\sin(\theta)\,, \tag{45}$$

$$\frac{d\theta}{dt} = -\frac{\partial \tilde{H}}{\partial \eta} = 2AT_{1134}\cos(\theta)\,(D-2\eta) + (\Omega_1\eta + \Omega_0)\,A + \Delta_{11}^{34}, \tag{46}$$

where the Hamiltonian is given by Eq. (43). This configuration may be interpreted as the Benjamin-Feir instability in the presence of an additional non-resonant wave; although there is no energy exchange between the degenerate quartet and mode $\mathbf{k}_2$, the frequency corrections arising from the presence of an additional mode are sufficient to substantially alter the overall dynamics. The phase plane $\{(\eta,\theta) \mid \eta \in [0,D], \theta \in [-\pi,\pi)\}$ is a truncated cylinder with parametric dependence on B. If $B = 1$ the total wave action is in the non-resonant mode $\mathbf{k}_2$, while $B = 0$ corresponds to the absence of the non-resonant satellite, i.e. the classical Benjamin-Feir configuration explored by Andrade & Stuhlmeier [27].

The lower boundary $\eta = 0$ of the phase space corresponds to a non-resonant three-mode configuration, consisting of modes $\mathbf{k}_3, \mathbf{k}_4$ and the satellite $\mathbf{k}_2$. The upper boundary $\eta = D$ corresponds to a bichromatic sea consisting of modes $\mathbf{k}_1$ and the satellite $\mathbf{k}_2$. The latter is the classical setting for the Type Ib instability, which arises from a linear stability analysis (see Leblanc [25]). To relate the configuration to physical wave parameters, the total wave action is obtained from the steepness of the waves $\mathbf{k}_1$ and $\mathbf{k}_2$ by means of Eq. (21).

Akin to Type Ia, we find four classes of fixed points as shown in Table 2. The set of Type Ib equations describes an interacting degenerate quartet and a fourth, non-interacting wave $\mathbf{k}_2$. The degenerate quartet itself exhibits instabilities (discussed in detail in [27]), while the addition of a fourth wave engenders a shift in the frequencies (dispersion correction) through the symmetric interaction kernels T_{ijij} and the Stokes' corrections Γ_i.

Fig. 6 shows the regions where the four types of fixed points exist, for a principal wave $\mathbf{k}_1 = (1,0)$, which, in the absence of other waves, corresponds to a steepness $\epsilon = 0.2$. The parameter space (k_x, k_y) maps out the possible degenerate quartets $\mathbf{k}_3 = (1+k_x, k_y)$ and $\mathbf{k}_4 = (1-k_x, -k_y)$, which are usually considered in the context of the Benjamin-Feir instability. The non-resonant wave $\mathbf{k}_2 = (\cos(\phi), \sin(\phi))$ subtends an angle ϕ with the primary (or carrier) wave $\mathbf{k}_1$, and may be allocated some of the total energy by modifying the parameter D (in this case $D = 0.5$).

The planar Hamiltonian structure of the dynamical system again makes it simple to classify the fixed points, exactly as in Section 2.2. Here the Jacobi determinant at the top ($\eta = D$) and bottom ($\eta = 0$) boundaries is $\det(J) = -4A^2D^2T_{1134}^2\sin^2(\theta)$, indicating that fixed points with $\det(J) \neq 0$ on these boundaries are saddle points. Investigating the fixed points at $\eta = D$ (see Table 2), we find that the Jacobi determinant there evaluates to

$$\det(J) = (\Delta_{11}^{34} + 2\Gamma_1 - \Gamma_3 - \Gamma_4)^2 - 4T_{1134}^2|b_1|^4, \tag{47}$$

and the condition for the existence of saddle points $\det(J) < 0$ coincides exactly with the instability condition derived from linearisation by Leblanc [25, Eq. (10)].

Thus, as discussed for Type Ia instability in Section 2.2, the appearance of distinct fixed points at $\eta = D$ through a zero-eigenvalue bifurcation destroys the stability of the bichromatic waves on the nullcline. The appearance of these saddle points implies existence of a heteroclinic connection, which is identified with a discrete breather solutions of the four-wave Zakharov equation. They represent modifications of the Type Ib discrete breathers explored recently by Andrade & Stuhlmeier [27]. The phase portraits are similar in appearance to those found for the Benjamin-Feir instability therein (see Fig. 1, [27]), albeit restricted to a phase-space ranging from $\eta = [0, D]$, and are not plotted here.

The interior fixed points at $\theta = 0, \pm\pi$ are steady state quartets of waves subject to the Type Ib resonance condition. The domains in parameter space where such fixed points occur are given in Fig. 4 for a particular choice of carrier steepness $\epsilon = 0.25$, satellite energy fraction $D = 0.5$, and three values of satellite wave inclination $\phi = 0, \pi/2$ and π (i.e. the satellite is collinear, orthogonal, or propagating counter to the carrier $\mathbf{k}_1$).

3. The discrete Hamiltonian for five-wave interactions

If we extend the weakly nonlinear theory to include quartically nonlinear terms, these naturally give rise to the possibility of resonant interactions of quintets of waves. Such interactions, which arise on a slower time-scale and have a smaller contribution – by a factor of ϵ – than the dominant (cubically nonlinear) quartet interactions nevertheless play an important role in some physical phenomena. For some regions of parameter space the lower-order instabilities may not be active (see e.g. the regions plotted in Figs. 3, 4, and 6), meaning that the weaker quintet instabilities dominate. In particular, quintet instabilities have been implicated in the formation of horseshoe shaped patterns observed in wind-driven seas [13,18]. The Hamiltonian formulation for the weakly nonlinear problem including quartic terms was given by Krasitskii [31, Eq. (2.24)], and forms the cornerstone of our analysis.

Perhaps the simplest case where quintet interaction takes place is in a wave field with three modes $\mathbf{k}_1, \mathbf{k}_2$ and $\mathbf{k}_3$ satisfying the degenerate quintet resonance condition $3\mathbf{k}_1 = \mathbf{k}_2 + \mathbf{k}_3$. For this case the Hamiltonian, in amplitude-phase variables is

$$\begin{aligned}H(|b_i|^2, \phi_i) = &\sum_{i=1}^{3}\omega_i|b_i|^2 + \frac{1}{2}\sum_{i,j=1}^{3}e_{ij}T_{ij}|b_i|^2|b_j|^2 \\ &+ 2\tilde{W}_{23111}^{(2)}\sqrt{|b_2|^2|b_3|^2|b_1|^6}\cos(3\phi_1 - \phi_2 - \phi_3),\end{aligned} \tag{48}$$

Table 2
Fixed points for the Type Ib instability (41)–(42). Each row depicts a fixed point, with corresponding value of amplitude parameter η (column 1), dynamic phase θ (column 2), and value of the Hamiltonian $\tilde{H}$ (column 3).

η	θ	$\tilde{H}$
0	$\pm\arccos\left(\frac{A\Omega_0+\Delta_{11}^{34}}{2ADT_{1134}}\right)$	0
D	$\pm\arccos\left(\frac{A\Omega_1 D+A\Omega_0+\Delta_{11}^{34}}{2ADT_{1134}}\right)$	$-\frac{\left((\Omega_1 D+2\Omega_0)A+2\Delta_{11}^{34}\right)D}{2}$
$\frac{2ADT_{1134}-A\Omega_0-\Delta_{11}^{34}}{A(\Omega_1+4T_{1134})}$	$\pm\pi$	$\frac{\left(2ADT_{1134}-A\Omega_0-\Delta_{11}^{34}\right)^2}{(2\Omega_1+8T_{1134})A}$
$-\frac{2ADT_{1134}+A\Omega_0+\Delta_{11}^{34}}{A(\Omega_1-4T_{1134})}$	0	$-\frac{\left(2ADT_{1134}+A\Omega_0+\Delta_{11}^{34}\right)^2}{(-2\Omega_1+8T_{1134})A}$

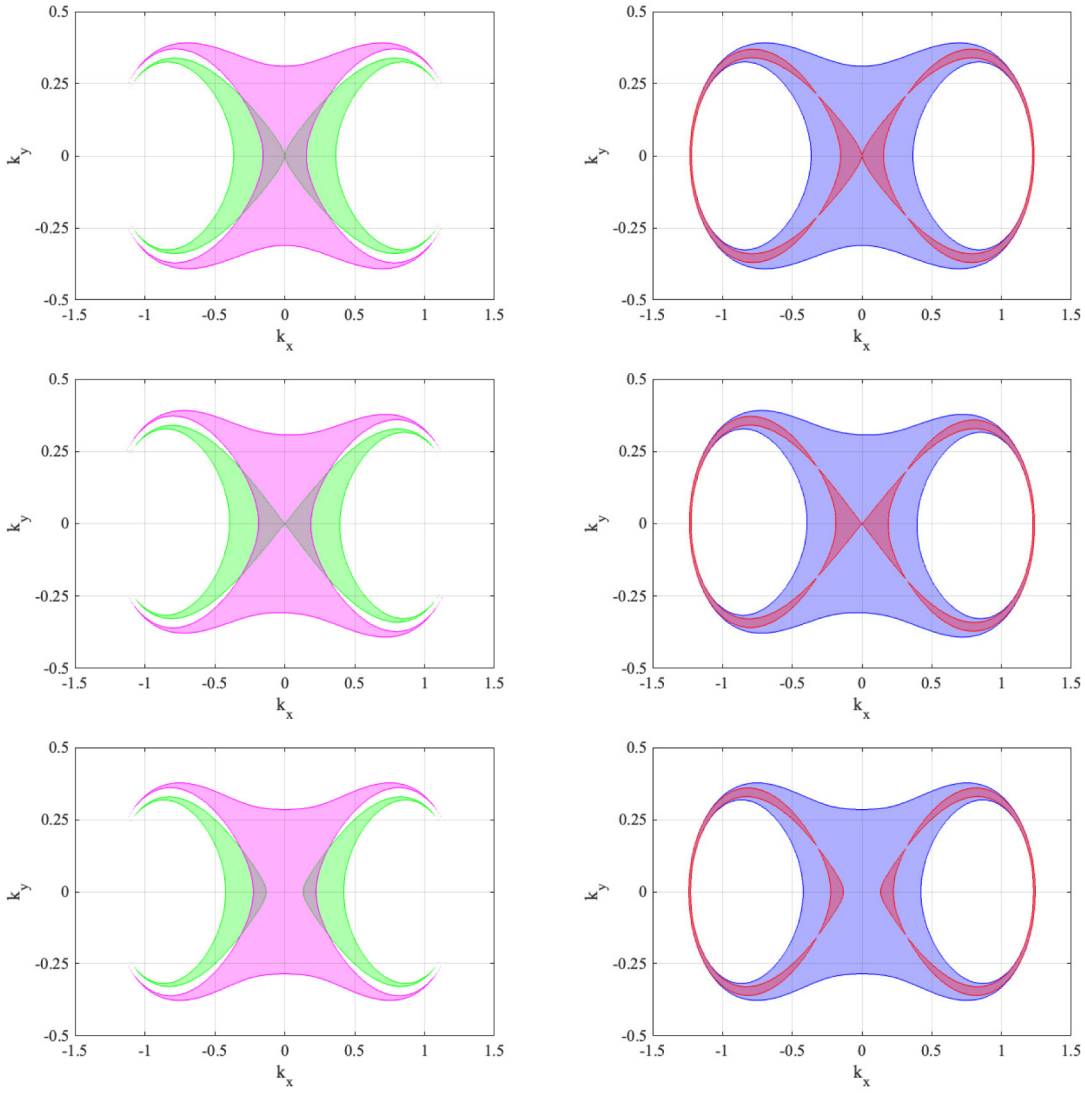

Fig. 6. Appearance of fixed points for Class Ib instabilities for $\epsilon = 0.25$, $D = 0.5$, and $\phi = 0$ (top panels), $\phi = \pi/2$ (middle panels) and $\phi = \pi$ (bottom panels). Left panels show fixed points at $\eta = D$ (green domain) and $\eta = 0$ (magenta domain). Right panels show fixed points at $\theta = 0$ (blue domain) and $\theta = \pm\pi$ (red domain). (For interpretation of the references to colour in this figure legend, the reader is referred to the web version of this article.)

where the five-wave interaction kernels are computed from the formulas obtained by [31], and T_{ij} are the symmetric four-wave kernels used extensively in Section 2. Since no other non-trivial resonant interactions occur, we write $W = \tilde{W}^{(2)}_{23111}$ for brevity.

The corresponding discrete Zakharov equation is

$$\frac{d|b_1|^2}{dt} = -\frac{\partial H}{\partial \phi_1} = 6W\sqrt{|b_2|^2|b_3|^2|b_1|^6}\sin(3\phi_1-\phi_2-\phi_3), \tag{49}$$

$$\frac{d|b_{2,3}|^2}{dt} = -\frac{\partial H}{\partial \phi_1} = -2W\sqrt{|b_2|^2|b_3|^2|b_1|^6}\sin(3\phi_1-\phi_2-\phi_3), \tag{50}$$

$$\frac{d\phi_1}{dt} = \frac{\partial H}{\partial |b_1|^2} = \omega_1+\Gamma_1+3W\sqrt{|b_2|^2|b_3|^2|b_1|^2} \times \cos(3\phi_1-\phi_2-\phi_3), \tag{51}$$

$$\frac{d\phi_2}{dt} = \frac{\partial H}{\partial |b_2|^2} = \omega_2 + \Gamma_2 + W\sqrt{\frac{|b_3|^2}{|b_2|^2}|b_1|^6} \times \cos(3\phi_1 - \phi_2 - \phi_3), \tag{52}$$

$$\frac{d\phi_3}{dt} = \frac{\partial H}{\partial |b_3|^2} = \omega_3 + \Gamma_3 + W\sqrt{\frac{|b_2|^2}{|b_2|^3}|b_1|^6} \times \cos(3\phi_1 - \phi_2 - \phi_3). \tag{53}$$

3.1. Hamiltonian formulation of Type IIb instability

In contrast to the cubically nonlinear case which exhibits three conserved quantities, the quartically nonlinear system conserves total energy (in the form of the Hamiltonian) and momentum only, but not wave action. However, for three modes the conservation of the two components (x, y) of the momentum

$$\mathbf{M} = \mathbf{k}_1|b_1|^2 + \mathbf{k}_2|b_2|^2 + \mathbf{k}_3|b_3|^2, \tag{54}$$

is sufficient to determine the possible energy transfers, and find an auxiliary amplitude parameter in a fashion analogous to that pursued in (12)–(13). In this case the system of two equations has rank 2, and we ultimately write the magnitudes as

$$|b_1|^2 = A\eta, \tag{55}$$

$$|b_2|^2 = A(1-\eta)/3, \tag{56}$$

$$|b_3|^2 = A(1-\eta)/3. \tag{57}$$

Here η is between 0 and 1 and this particular solution is chosen so that the wave momentum vector $\mathbf{M} = A\mathbf{k}_1$. Note that A is not the total wave action, but simply a positive scalar. Without loss of generality we take $\mathbf{k}_1 = (1, 0)$, so that $\mathbf{M} = (A, 0)$.

3.2. Dynamics of Type IIb instability

We can exploit the discrete Hamiltonian structure to recast our system in the phase plane. As before, we introduce a dynamic phase

$$\theta = 3\phi_1 - \phi_2 - \phi_3, \tag{58}$$

that allows us to reduce the Hamiltonian structure to a simpler Hamiltonian system in the new variables η and θ, as pursued for Type Ia in Section 2.1 and Ib in Section 2.3. The reduced Hamiltonian and the corresponding equations of motion are:

$$\tilde{H}(\eta,\theta) = -2WA^{3/2}\eta^{3/2}(1-\eta)\cos(\theta) - (\Delta_{111}^{23} + A\Omega_0)\eta - \frac{A\Omega_1}{2}\eta^2, \tag{59}$$

$$\frac{d\eta}{dt} = 2WA^{3/2}\eta^{3/2}(1-\eta)\sin(\theta), \tag{60}$$

$$\frac{d\theta}{dt} = \Delta_{111}^{23} + A\Omega_0 + A\Omega_1\eta + WA^{3/2}\eta^{1/2}(3-5\eta)\cos(\theta). \tag{61}$$

The coefficients Ω_0 and Ω_1 come from the linear polynomial

$$3\Gamma_1 - \Gamma_2 - \Gamma_3 = A\Omega_0 + A\Omega_1\eta, \tag{62}$$

which can be found in Appendix A and the frequency detuning is $\Delta_{111}^{23} = 3\omega_1 - \omega_2 - \omega_3$.

Once again the parameter A is related to the steepness of the wave $\mathbf{k}_1$ as

$$A = 2\pi^2\frac{\omega_1}{k_1^3}\epsilon_1^2. \tag{63}$$

An analogous planar system was found by [21, Eq. (2.19)] in their study of water wave horseshoe patterns, with the additional minor restriction of equal side-band phases $\phi_2 = \phi_3$. These authors subsequently added forcing and dissipation terms to the system in order to recover the forward-oriented wave fronts observed experimentally for crescent wave patterns (see the discussion by [13,38]).

3.2.1. Fixed points and heteroclinic connections

The dynamics of the type IIb instability are similar to those of the type Ia instability described before. The Hamiltonian structure of the planar system implies that the Jacobi matrix has vanishing trace and that its eigenvalues are $\lambda_{1,2} = \pm\sqrt{-\det(J)}$, which ensures that all fixed points are either centres or saddles.

The system (60)–(61) admits the following fixed points:

$$\eta = 1, \quad \theta_1 = \pm\arccos\left(\frac{\Delta_{111}^{23} + A\Omega_0 + A\Omega_1}{2A^{3/2}W}\right), \tag{64}$$

provided that the expression in the argument of the arccos is between -1 and 1. These are fixed points along the contour of plane Stokes' waves, corresponding to the 'trivial' stationary state (3.2b) in [21]. A second type of fixed point of the form $(\eta, \theta) = (\eta_0, 0)$ is found whenever η_0 is a solution of the equation

$$\Delta_{111}^{23} + A\Omega_0 + A\Omega_1\eta + WA^{3/2}\eta^{1/2}(3-5\eta) = 0. \tag{65}$$

These correspond to the "in-phase" nontrivial stationary states found by [39] and [21, Eq. (3.3a)]. A third type of fixed point appears at $(\eta, \theta) = (\eta_\pi, \pm\pi)$ where η_π solves the equation

$$\Delta_{111}^{23} + A\Omega_0 + A\Omega_1\eta - WA^{3/2}\eta^{1/2}(3-5\eta) = 0. \tag{66}$$

Note the change of sign before the kernel; these fixed points are the "out-of-phase" stationary states in [21, Eq. (3.3b)]. In general, and unlike the configuration of the type I instabilities, the type IIb does not admit fixed points at $\eta = 0$.

The reduced Hamiltonian $\tilde{H}$ is constant along the line $\eta = 1$ where any solution represents a single Stokes' wave with all the energy concentrated in the mode $\mathbf{k}_1$. The appearance of fixed points at $\eta = 1$ changes the stability of this nullcline. Indeed there are two distinct fixed points on $\eta = 1$, symmetric with respect to $\theta = 0$, when

$$\left(\frac{\Delta_{111}^{23}}{2} + \frac{A}{2}(3T_{aaaa} - 2T_{abab} - 2T_{acac})\right) - A^3W^2 < 0. \tag{67}$$

At each of those points the Jacobi matrix is

$$J = \begin{pmatrix} -2A^{3/2}W\sin(\theta_1) & 0 \\ -6A^{3/2}W\cos(\theta_1) + A\Omega 1 & 2A^{3/2}W\sin(\theta_1) \end{pmatrix}, \tag{68}$$

which immediately shows that both fixed points are saddles. Note that Eq. (67) is equivalent to $\det(J) < 0$. This equation is exactly the classical linear stability criterion, obtained in equation (3.8) of [19]. Distinct fixed points at $\eta = 1$ are always connected by a heteroclinic solution when Eq. (67) is satisfied and this implies the orbital instability of the solutions at $\eta = 1$.

For a given value of total wave action the dynamics of the quintet can be classified according to the types of fixed points that it may have, and we identify the regions where different fixed points occur in parameter space. In Fig. 7, we take $\epsilon_1 = 0.41$ and a (degenerate) quintet of the form $k_1 = (1, 0)$, $k_2 = k_1 + (k_x, k_y)$ and $k_3 = 2k_1 - (k_x, k_y)$. We plot regions in the (k_x, k_y) plane where different fixed points occur. The blue region (panels a and d) is the region where fixed points at $\eta = 1$ exist, and coincides with the instability region of [19]. The yellow region (panels b and d) corresponds to fixed points at $\theta = 0$, i.e. centres, and the red region (panels c and d) to fixed points at $\theta = \pm\pi$, i.e. saddle points.

Note that the blue region is a subset of the yellow region. This means that fixed points at $\eta = 1$ are accompanied by fixed point at $\theta = 0$. The red region on the other hand is not fully contained in the yellow region as can be seen in panel d near the point $k_x = 1.7$ and $k_y = 1$.

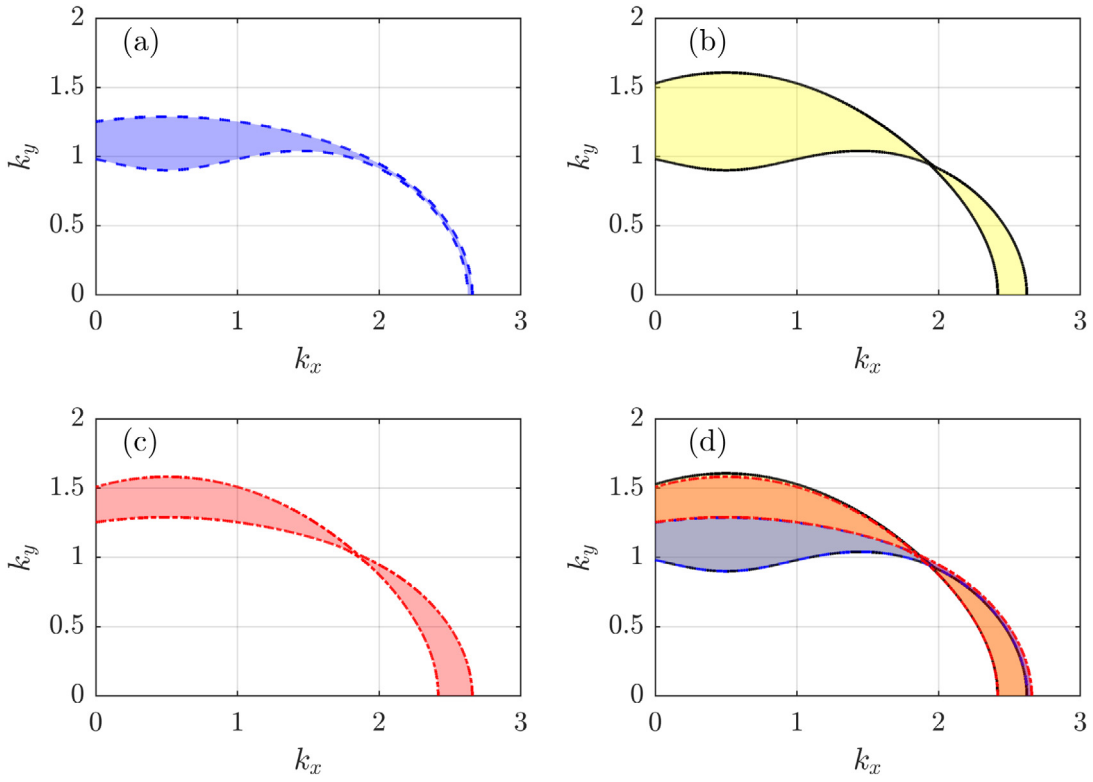

Fig. 7. Classification of the dynamics for $\epsilon_1 = 0.41$. Panel a: Region with fixed points of the form $(\theta_1, 1)$. Linearly unstable region. Panel b: Region with fixed points of the form $(0, \eta_0)$. Panel c: Region with fixed point of the form (π, η_π). Panel d: Union of the regions plotted in panels a (in blue), b (in yellow) and c (in red). (For interpretation of the references to colour in this figure legend, the reader is referred to the web version of this article.)

3.2.2. Type IIb discrete breathers

Saddle points of the Type IIb system appear with separatrices connecting them. When these saddle points lie on $\eta = 1$ (corresponding to plane Stokes waves), the heteroclinic connection corresponds to a novel fourth-order Akhmediev-type breather. Starting from a quintet with fixed points at $(1, -\theta_1)$ and $(1, \theta_1)$, we obtain in this section analytical expressions for such a breather.

We start with the following equation

$$2WA^{3/2}\eta^{3/2}\cos(\theta) = \Delta^{23}_{111} + A\Omega_0 + \frac{A\Omega_1}{2}(1+\eta), \tag{69}$$

which follows from equating the planar Hamiltonian (59) to its value at $\eta = 1$. Then, by means of implicit differentiation, whereby η is regarded as a function of θ instead of t, we obtain the following equation:

$$\frac{d\eta}{d\theta} = \frac{\eta^{3/2}\sin(\theta)}{\frac{3}{2}\eta^{1/2}\cos(\theta) - \frac{\Omega_1}{4A^{1/2}W}}. \tag{70}$$

Direct integration of Eq. (70) yields the following relation between η and θ:

$$C - \eta^{3/2}\cos(\theta) + \frac{\Omega_1}{4A^{1/2}W}\eta = 0, \tag{71}$$

where the integration constant C is determined from the condition that $\lim_{\theta\to\theta_1}\eta = 1$. Its value is

$$C = \frac{\Delta^{23}_{111} + A\Omega_0 + A\Omega_1/2}{2A^{3/2}W}. \tag{72}$$

Eq. (71) can be used to plot the trajectory in phase space.

In order to find the solution of the Hamiltonian system (60) and (61) the following equation for the dynamic phase has to be solved

$$\frac{d\theta}{dt} = WA^{3/2}\eta^{1/2}(3-\eta)\cos(\theta) - 2A^{3/2}W\cos(\theta_1). \tag{73}$$

Once its solution is obtained it is used in combination with Eq. (71) to obtain the time evolution of the amplitudes.

In Fig. 8 we plot the dynamics for a case with $\epsilon_1 = 0.41$, $k_x = 0.5$ and $k_y = 1.28$. The fixed points appearing in this case can be read off from Fig. 7, which is plotted for the same value of wave slope: this case corresponds to two saddle points at $\eta = 1$ (blue region, panel (a) in Fig. 7), and a centre at $\theta = 0$ (yellow region, panel (b) in Fig. 7). These fixed points are shown in the upper panel of Fig. 8, which depicts the phase portrait with heteroclinic orbit.

The middle panel of Fig. 8 shows the (dimensionless) time evolution of the amplitudes along the heteroclinic orbit obtained from Eqs. (70) and (73). The blue line corresponds to the carrier wave $\mathbf{k}_1$ and the red line to side bands $\mathbf{k}_2$ and $\mathbf{k}_3$. Recall that there is equipartition in the initial side-band magnitudes, but no conservation of wave action. The time scale used in the figure is $\tilde{t} = t/(2WA^{3/2})$.

The lower panel in Fig. 8 shows a snapshot of the free surface elevation at $t = 0$, the moment of maximum modulation. In order to compute the complex envelope (from which the free surface follows by taking its real part) values of the individual phases must be assigned in such a way that the dynamic phase vanishes. The values used are $\phi_1 = 0$, $\phi_2 = \pi$ and $\phi_3 = -\pi$. The vertical scale in the figure is $\tilde{z} = z/\epsilon_1$, while the horizontal variables have been nondimensionalised as $\tilde{x} = x|\mathbf{k}_1|$ and $\tilde{y} = y|\mathbf{k}_1|$ with $\mathbf{k}_1 = (1, 0)$. As $\tilde{t}$ tends to $\pm\infty$, this three-dimensional, modulated wave train returns to the monochromatic (Stokes' wave) background.

3.3. Type IIc instability

For three waves $\mathbf{k}_1$, $\mathbf{k}_2$ and $\mathbf{k}_3$ the quintet resonance condition can be fulfilled when $3\mathbf{k}_1 = \mathbf{k}_2 + \mathbf{k}_3$, or when $\mathbf{k}_1 + 2\mathbf{k}_2 = 2\mathbf{k}_3$. In the latter case – which we term Type IIc, – conservation of momentum can also be used to reduce the governing equations to

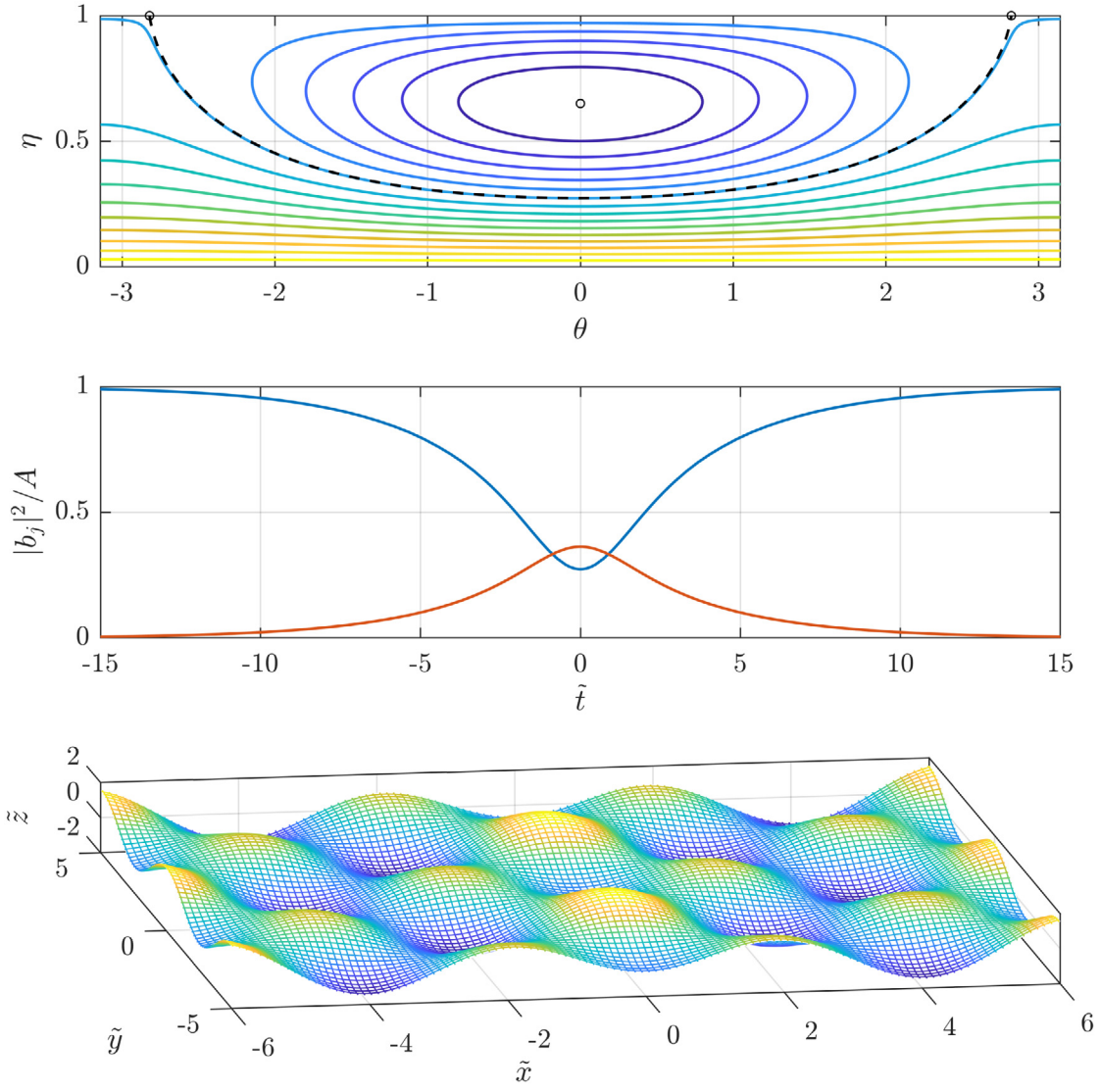

Fig. 8. Class II instabilities. Upper panel: Level lines of the Hamiltonian. The red line is the discrete (1-1) breather solution. Black circles are the fixed point of the dynamical system. Middle panel: Time evolution of $|b_1|^2$ in blue. Evolution of $|b_2|^2 = |b_3|^2$ in red. Wave action was normalised by A. The time scale is $\tilde{t} = t/(2WA^{3/2})$. Lower panel: Free surface elevation at $\tilde{t} = 0$. (For interpretation of the references to colour in this figure legend, the reader is referred to the web version of this article.)

a planar dynamical system. The classes of fixed points are similar, and full details are provided in Appendix C.

From a physical perspective there are two important cases: if only mode $\mathbf{k}_3$ is present the wave field is monochromatic. In this case there are no fixed points in the system, and the solution is always stable to perturbations of the form $\mathbf{k}_1 + 2\mathbf{k}_2 = 2\mathbf{k}_3$. The complementary case is for an initial bichromatic wave train consisting of $\mathbf{k}_1$ and $\mathbf{k}_2$. In this case it is possible to find fixed points and heteroclinic orbits, i.e. the bichromatic wave train is unstable to particular monochromatic perturbations.

As we have seen in previous sections, the stability properties are completely determined by the existence of fixed points. Analogous methods enable us to classify the fixed points for a triad of waves of the form $\mathbf{k}_1 = (k_x, k_y)$, $\mathbf{k}_2 = (1 - k_x/2, -k_y/2)$ and $\mathbf{k}_3 = (1, 0)$ with total momentum $\mathbf{M} = (A, 0)$ with $A = 3.31$ exactly as for the type IIb case – these are depicted in Fig. C.9 in Appendix C. While this configuration corresponds to $\epsilon_3 = 0.41$, the structure of the resonance condition implies that the fixed points exist only when ϵ_1 and ϵ_2 are in excess of 1. This is physically unrealistic, and the Type IIc instability of a bichromatic wave train is thus only of mathematical interest.

4. Discussion and conclusions

We have undertaken to investigate the three classical instabilities of waves on the surface of deep water from the perspective of dynamical systems. In the classical treatment, these instabilities are treated via linearisation [19,25]: in Type Ib and Type IIb the discrete equations are linearised about a monochromatic solution, while in Type Ia the discrete equations are linearised about a bichromatic solution. Because the underlying set of discrete equations comes from a reduced Hamiltonian formulation, it is possible to exploit this, together with other conservation laws, to classify the full dynamics.

A key ingredient in our approach is the fact that a single resonant set is governed by one dynamic phase: this condenses the evolution of the phases into a single equation, rather than following each modal phase separately. The second important idea is to use momentum (and, for quartet resonances, wave action) conservation, together with the wavenumber resonance condition, to inform the choice of amplitude parameter. If we wish to describe a scenario where a monochromatic basic state is perturbed, say, the total momentum must always coincide

with that of the basic state. The second variable in the planar description, namely the amplitude parameter, follows naturally from this choice.

In the three cases considered the phase plane is the surface of a truncated cylinder, with the dynamic phase taking values between $-\pi$ and π, and different values of height depending on the configuration. In all cases, the basic state – either a monochromatic wave or a bichromatic wave – is found on the top of the cylinder. The converse of this – when all the momentum has been transferred away from the basic state – are the solutions at the bottom of the cylinder. Trajectories, which are the level lines of the Hamiltonian, wind around the phase space in periodic orbits, which can be confined by separatrices connecting fixed points of the system.

As mentioned above, when such fixed points occur on the top of the phase plane, they signal orbital instability of the basic state. We have shown that the existence criteria for distinct fixed points are algebraically identical with the instability thresholds obtained classically from linearisation. Moreover, each pair of such fixed points is connected by a separatrix, which we identify with a breather or multibreather solution to the system in question. We have provided explicit solutions and plots of these new, discrete breather solutions for both quartet and quintet instabilities. These include special cases where one bichromatic wave train undergoes modulation and ultimately transforms into a different bichromatic wave train, a special case of a Type Ia multibreather.

The nature of our phase-plane approach also makes clear the relationship between energy exchange and phase-coherence. Roughly speaking, energy is the vertical coordinate and phase the horizontal (or angular) coordinate in our phase portraits. When significant energy exchange is taking place, trajectories are nearly vertical, implying that the phase is nearly coherent, and vice versa. Interior fixed points are a special case: these configurations are steady-state resonances or near-resonances, where phase and energy do not change with time. Such steady solutions, obtained using the so-called homotopy analysis method, have been the subject of considerable recent interest [37,40].

The approach presented is quite general, and could potentially be extended to other isolated resonances of six or more waves. Additionally, it is always possible to add non-resonant contributions to any isolated resonance; the template for such a case is the Type Ib instability, which involves a single non-resonant satellite added to the Benjamin-Feir instability. Such non-resonant modes do not exchange energy, and therefore do not require a higher dimensional system. Their sole effect is via frequency corrections, which can be incorporated easily into the coefficients of the system.

Exploring how multiple resonances might be treated within the Hamiltonian framework is likely to be a challenge. Work by [11] has also identified a Type IIa instability consisting of four modes $\mathbf{k}_1 + \mathbf{k}_2 = 2\mathbf{k}_3 + \mathbf{k}_4$. Due to the lack of wave action conservation for quintet interaction, this case may require somewhat different techniques. Recent work has also been undertaken in the vein of Shrira et al. [21], incorporating forcing and dissipation into discrete systems based on the higher order nonlinear Schrödinger equation [41]. Numerous possibilities exist to extend these approaches to the instabilities discussed in the present paper. Future work may also treat the observability of the new breather solutions in wave-flume experiments, in line with recent work observing breather solutions of the NLS [42–44].

Declaration of competing interest

The authors declare that they have no known competing financial interests or personal relationships that could have appeared to influence the work reported in this paper.

Data availability

No data was used for the research described in the article.

Acknowledgements

The authors would like to thank the anonymous referees for their detailed and helpful comments which served to improve the manuscript. This work was supported by the Engineering & Physical Sciences Research Council (grant number EP/V012770/1).

Appendix A. Coefficients Ω_0 and Ω_1

Throughout this paper we have denoted by Ω_0 and Ω_1 certain combinations of the kernels depending on the instability under investigation. The full expression of the coefficients for each case is given below.

For Type Ia the coefficients are:

$$\begin{aligned}\Omega_0 &= T_{13} + T_{23} - T_{33}/2 - 2T_{43} + T_{14} + T_{24} - T_{44}/2,\\ \Omega_1 &= (T_{11} + 4T_{12} + T_{22}) + (T_{33} + 4T_{34} + T_{44})\\ &\quad - 4(T_{13} + T_{14} + T_{23} + T_{24}).\end{aligned}$$

For Type Ib the coefficients are:

$$\begin{aligned}\Omega_0 &= B\,(4T_{12} - 2T_{23} - 2T_{24})\\ &\quad + D\left(2T_{14} - \frac{T_{44}}{2} + 2T_{13} - \frac{T_{33}}{2} - 2T_{34}\right),\\ \Omega_1 &= 2T_{11} + \frac{1}{2}T_{33} + \frac{1}{2}T_{44} + 2T_{34} - 4T_{13} - 4T_{14}.\end{aligned}$$

Here B and D are parameters which determine what fraction of the total wave action A is contained in the resonant degenerate quartet, and what fraction is contained in the non-resonant satellite wave. When $B = 0$ the non-resonant satellite is absent entirely, and this recovers the expressions derived for the Benjamin-Feir instability by [27, cf. Eq. (2.12-2.13)].

Lastly, for type IIb the coefficients are:

$$\begin{aligned}\Omega_0 &= 2T_{12} + 2T_{13} - (T_{22} + 4T_{23} + T_{33})/3,\\ \Omega_1 &= 3T_{11} - 4(T_{12} + T_{13}) + (T_{22} + T_{33} + 4T_{23})/3.\end{aligned}$$

Appendix B. Type Ia instability with side-band imbalance

This section shows how the calculations given in Section 2.1 can be extended to account for unequal initial magnitudes, i.e. a lack of equidistribution of wave action among modes $\mathbf{k}_1$ and $\mathbf{k}_2$. Setting

$$\alpha = \frac{|b_1(0)|^2 - |b_2(0)|^2}{A}$$

we find from conservation of wave action (12) for the initial configuration ($|b_1(0)|^2 + |b_2(0)|^2 = A$) that

$$\frac{|b_1(0)|^2}{A} = \frac{1+\alpha}{2}, \quad \frac{|b_2(0)|^2}{A} = \frac{1-\alpha}{2}. \tag{B.1}$$

Therefore, in the vein of our previous argument we have a single amplitude parameter, which we here call $g(t)$, as follows

$$\begin{aligned}&|b_1(t)|^2 = A\left(\frac{1+\alpha}{2} - g(t)\right),\ |b_2(t)|^2 = A\left(\frac{1-\alpha}{2} - g(t)\right),\\ &|b_3(t)|^2 = |b_4(t)|^2 = Ag(t).\end{aligned}$$

Of course, other choices are possible, provided we remain in the kernel of the matrix K given by the resonance condition (13). The

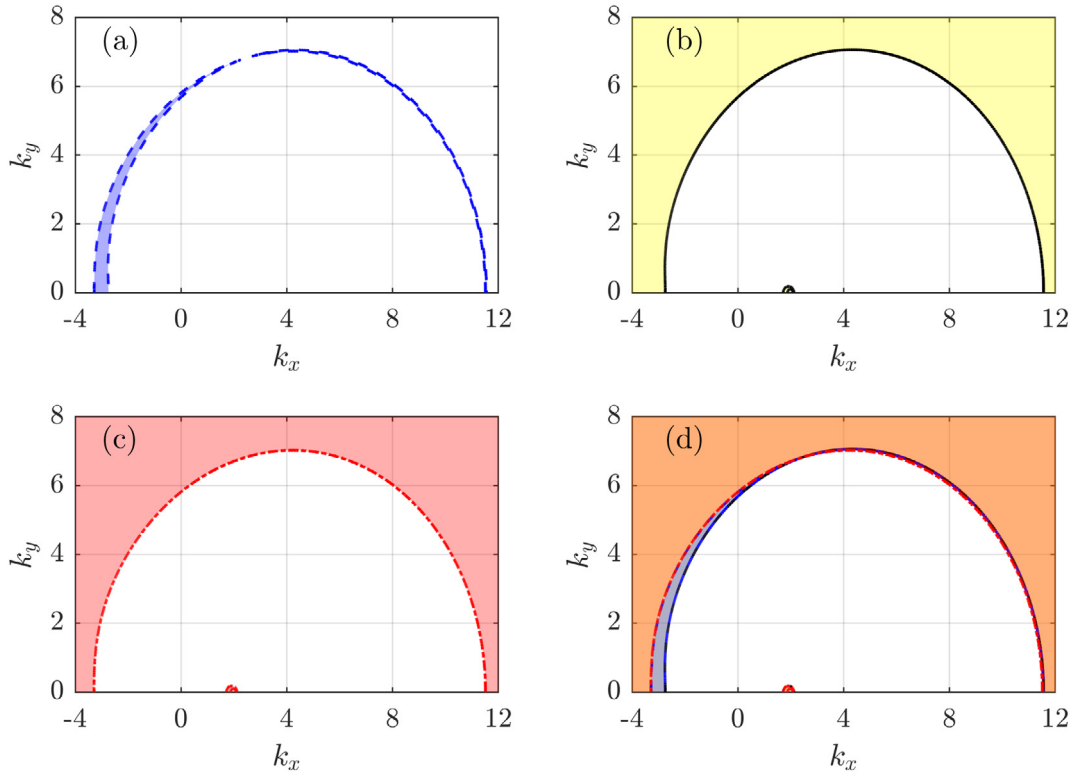

Fig. C.9. Classification of the dynamics for $\epsilon_3 = 0.41$. Panel a: Region with fixed points of the form $(\theta_{1/2}, 1/2)$. Panel b: Region with fixed points of the form $(0, \eta_0)$. Panel c: Region with fixed point of the form (π, η_π). Panel d: Union of the regions plotted in panels a (in blue), b (in yellow) and c (in red). (For interpretation of the references to colour in this figure legend, the reader is referred to the web version of this article.)

planar system associated with the auxiliary variables $g(t)$ and $\theta(t)$ is then

$$g'(t) = -2TA^2\sqrt{(-1-\alpha+2\,g)(-1+\alpha+2\,g)g^2}\,\sin(\theta), \tag{B.2}$$

$$\theta'(t) = \Delta + \Gamma_1 + \Gamma_2 - \Gamma_3 - \Gamma_4 - \frac{2TA\left(\alpha^2 - 8g^2 + 6\,g - 1\right)\cos(\theta)}{\sqrt{(-1-\alpha+2\,g)\,(-1+\alpha+2\,g)}}, \tag{B.3}$$

where the initial modes $\mathbf{k}_1$, $\mathbf{k}_2$ are found at $g = 0$ and the other limit of the phase space is reached when $g = \min\{\frac{1+\alpha}{2}, \frac{1-\alpha}{2}\}$. Thus, while the bottom boundary of the phase space consists of the initial, bichromatic sea the maximum energy exchange which can be obtained occurs when the energetically smaller of modes $|b_1|$ and $|b_2|$ has completely depleted – this means that the upper boundary of the phase space consists of three modes rather than two.

To return to the linear stability threshold obtained by Leblanc [25], we find that the Jacobi determinant of the system (B.2)–(B.3) at the initial configuration $g = 0$ is

$$\det(J) = -4T^2A^2(1-\alpha^2) + (\Delta + \Gamma_1 + \Gamma_2 - \Gamma_3 - \Gamma_4),$$

which recovers Leblanc's result (15) when α is substituted from Eq. (B.1) above.

Appendix C. Specifics of Type IIc instability

As noted in Section 3, in addition to the case with $3\mathbf{k}_1 = \mathbf{k}_2 + \mathbf{k}_3$ an additional form of quintet resonance with three modes satisfying $\mathbf{k}_1 + 2\mathbf{k}_2 = 2\mathbf{k}_3$ is possible. In this case the Hamiltonian is

$$H(|b_i|^2, \phi_i) = \sum_{i=1}^{3}\omega_i|b_i|^2 + \frac{1}{2}\sum_{i,j=1}^{3}e_{ij}T_{ij}|b_i|^2|b_j|^2 + 3\tilde{W}^{(2)}_{33122}|b_2|^2|b_3|^2\sqrt{|b_1|^2}\cos(\phi_1 + 2\phi_2 - 2\phi_3). \tag{C.1}$$

Once again without risk of confusion we denote $W = \tilde{W}^{(2)}_{33122}$ and $\Delta = \Delta^{33}_{122} = \omega_1 + 2\omega_2 - 2\omega_3$.

Owing to conservation of momentum we can introduce a parameter η so that

$$|b_1|^2 = A\eta, \tag{C.2}$$

$$|b_2|^2 = 2A\eta, \tag{C.3}$$

$$|b_3|^2 = 2A(1/2 - \eta). \tag{C.4}$$

Here η is between 0 and 1/2. Without loss of generality the momentum is chosen to be $\mathbf{M} = A\mathbf{k}_3 = (A, 0)$.

We introduce the dynamic phase

$$\theta = \phi_1 + 2\phi_2 - 2\phi_3, \tag{C.5}$$

allowing us to find a planar Hamiltonian for η and θ. The planar Hamiltonian is

$$\tilde{H}(\theta, \eta) = -6WA^{3/2}\eta^{3/2}(1-2\eta)\cos(\theta) - (\Delta^{33}_{122} + A\Omega_0)\eta - \frac{A\Omega_1}{2}\eta^2, \tag{C.6}$$

with the coefficients Ω_0 and Ω_1 coming from the polynomial

$$\Gamma_1 + 2\Gamma_2 - 2\Gamma_3 = A\Omega_0 + A\Omega_1\eta, \tag{C.7}$$

and equations of motion given by

$$\frac{d\eta}{dt} = \frac{\partial\tilde{H}}{\partial\theta} = 6WA^{3/2}\eta^{3/2}(1-2\eta)\sin(\theta). \tag{C.8}$$

$$\frac{d\theta}{dt} = -\frac{\partial\tilde{H}}{\partial\eta} = \Delta^{33}_{122} + A\Omega_0 + A\Omega_1\eta + 3WA^{3/2}\eta^{1/2}(3-10\eta)\cos(\theta). \tag{C.9}$$

Analogous to the treatment of the Type IIb instability, fixed points exist when

$$\eta = \frac{1}{2} \text{ and } \theta = \arccos\left(\frac{\left(2A\Omega_0 + A\Omega_1 + 2\Delta^{33}_{122}\right)\sqrt{2}}{12\ WA^{\frac{3}{2}}}\right) \tag{C.10}$$

or else when $\theta = 0, \pm\pi$ and η is a root of

$$\Delta^{33}_{122} + A\Omega_0 + A\Omega_1\eta + 3WA^{3/2}\eta^{1/2}(3-10\eta) = 0.$$

In Fig. C.9 each of the regions indicate the existence different types of fixed points for a triad of the form $\mathbf{k}_3 = (1, 0)$, $\mathbf{k}_1 = (k_x, k_y)$ and $\mathbf{k}_2 = (1 - k_x/2, -k_y/2)$ in the (k_x, k_y) plane. The thin blue region (panel a) shows the existence of fixed points at $\eta = 1/2$. The existence of such fixed points should be interpreted as an instability of an underlying bichromatic sea with modes $\mathbf{k}_1$ and $\mathbf{k}_2$ (recall that when $\eta = 1/2$ in (C.2)–(C.4) only waves $\mathbf{k}_1$ and $\mathbf{k}_2$ are present) to monochromatic perturbations $\mathbf{k}_3$. The yellow region (panel b) corresponds to fixed points at $\theta = 0$ and the red region (panel c) to fixed points at $\theta = \pm\pi$. In the last panel (panel d) all the regions are plotted together, showing that the blue region corresponds to the difference between the yellow and red regions. Note that the regions in panels b and c are bounded for larger values of mode separation, i.e. large $\|(k_x, k_y)\|$.

With fixed points at $\eta = 1/2$ there is a heteroclinic orbit which describes a multibreather solution of the equations. Following step by step the procedure used for the type IIb instability the equations for the breather are

$$\frac{d\eta}{d\theta} = \frac{\eta^{3/2}\sin(\theta)}{\frac{3}{2}\eta^{1/2}\cos(\theta) - \frac{\Omega_1}{24A^{1/2}W}}, \tag{C.11}$$

and for the dynamic phase

$$\frac{d\theta}{dt} = 3WA^{3/2}\eta^{1/2}(3-2\eta)\cos(\theta) - 3\sqrt{2}WA^{3/2}\cos(\theta_{1/2}). \tag{C.12}$$

This solution tends, for $t \to \pm\infty$ to the bichromatic state $\mathbf{k}_1$, $\mathbf{k}_2$, while the modulation transfers some energy to the wave $\mathbf{k}_3$. As noted in Section 3.3 above, the steepness required to obtain fixed points at $\eta = 1/2$ – and a corresponding discrete multibreather – is physically unrealistic, so this should be treated as a mathematical solution only.

References

[1] O.M. Phillips, On the dynamics of unsteady gravity waves of finite amplitude part 1. The elementary interactions, J. Fluid Mech. 9 (2) (1960) 193–217.

[2] M.S. Longuet-Higgins, Resonant interactions between two trains of gravity waves, J. Fluid Mech. 12 (1962) 321–332.

[3] D.J. Benney, Non-linear gravity wave interactions, J. Fluid Mech. 14 (1962) 577–584.

[4] P.A.E.M. Janssen, Nonlinear four-wave interactions and freak waves, J. Phys. Oceanogr. 33 (4) (2003) 863–884.

[5] G. Akrish, R. Schwartz, O. Rabinovitch, Y. Agnon, Impact of extreme waves on a vertical wall, Nat. Hazards 84 (2) (2016) 637–653.

[6] D. Andrade, R. Stuhlmeier, M. Stiassnie, Freak waves caused by reflection, Coast. Eng. 170 (2021) 104004.

[7] M. Klein, M. Dudek, G.F. Clauss, S. Ehlers, J. Behrendt, N. Hoffmann, M. Onorato, On the deterministic prediction of water waves, Fluids 5 (1) (2020) 1–19.

[8] R. Stuhlmeier, M. Stiassnie, Deterministic wave forecasting with the Zakharov equation, J. Fluid Mech. 913 (2021) 1–22.

[9] V.E. Zakharov, L.A. Ostrovsky, Modulation instability: The beginning, Phys. D 238 (5) (2009) 540–548.

[10] C.C. Mei, M.A. Stiassnie, D.K.-P. Yue, Theory and Applications of Ocean Surface Waves, third ed., World Scientific Publishing Co., 2018.

[11] M. Ioualalen, C. Kharif, On the subharmonic instabilities of steady three-dimensional deep water waves, J. Fluid Mech. 262 (1994) 265–291.

[12] F. Dias, M. Hărăguş-Courcelle, On the transition from two-dimensional to three-dimensional water waves, Stud. Appl. Math. 104 (2) (2000) 91–127.

[13] D. Fructus, C. Kharif, M. Francius, Ø. Kristiansen, D. Clamond, J. Grue, Dynamics of crescent water wave patterns, J. Fluid Mech. 537 (2005) 155–186.

[14] O. Kimmoun, M. Ioualalen, C. Kharif, Instabilities of steep short-crested surface waves in deep water, Phys. Fluids 11 (6) (1999) 1679–1681.

[15] J.L. Hammack, D.M. Henderson, H. Segur, Progressive waves with persistent two-dimensional surface patterns in deep water, J. Fluid Mech. 532 (2005) 1–52.

[16] M. Okamura, Instabilities of weakly nonlinear standing gravity waves, J. Phys. Soc. Japan 53 (11) (1984) 3788–3796.

[17] J.W. McLean, Instabilities of finite-amplitude water waves, J. Fluid Mech. 114 (1982) 315–330.

[18] M.-Y. Su, Three-dimensional deep-water waves. part 1. experimental measurement of skew and symmetric wave patterns, J. Fluid Mech. 124 (1982) 73–108.

[19] M. Stiassnie, L. Shemer, On modification of the Zakharov equation for surface gravity waves, J. Fluid Mech. 143 (1984) 47–67.

[20] D.R. Fuhrman, P.A. Madsen, H.B. Bingham, Numerical simulation of lowest-order short-crested wave instabilities, J. Fluid Mech. 563 (2006) 415–441.

[21] V.I. Shrira, S.I. Badulin, C. Kharif, A model of water wave 'horse-shoe' patterns, J. Fluid Mech. 318 (5) (1996) 375–405.

[22] F. Collard, G. Caulliez, Oscillating crescent-shaped water wave patterns, Phys. Fluids 11 (11) (1999) 3195–3197.

[23] D.R. Fuhrman, P.A. Madsen, Potential dominance of oscillating crescent waves in finite width tanks, Phys. Fluids 17 (3) (2005) 038102.

[24] D. Lucas, M. Perlin, D.-Y. Liu, S. Walsh, R. Ivanov, M.D. Bustamante, Five-wave resonances in deep water gravity waves: Integrability, numerical simulations and experiments, Fluids 6 (6) (2021) 205.

[25] S. Leblanc, Stability of bichromatic gravity waves on deep water, Eur. J. Mech. B Fluids 28 (5) (2009) 605–612.

[26] S.I. Badulin, V.I. Shrira, C. Kharif, M. Ioualalen, On two approaches to the problem of instability of short-crested water waves, J. Fluid Mech. 303 (1995) 297–326.

[27] D. Andrade, R. Stuhlmeier, The nonlinear Benjamin-Feir instability - Hamiltonian dynamics, discrete breathers, and steady solutions, J. Fluid Mech. 958 (2023) A17, http://dx.doi.org/10.1017/jfm.2023.96.

[28] G. Cappellini, S. Trillo, Third-order three-wave mixing in single-mode fibers: exact solutions and spatial instability effects, J. Opt. Soc. Amer. B 8 (4) (1991) 824–838.

[29] T. Benzekri, C. Chandre, R. Lima, M. Vittot, A hamiltonian system for interacting benjamin–feir resonances, J. Phys. A: Math. Gen. 38 (24) (2005) 5381–5403.

[30] V.E. Zakharov, Stability of periodic waves of finite amplitude on the surface of a deep fluid, J. Appl. Mech. Tech. Phys. 9 (2) (1968) 190–194.

[31] V.P. Krasitskii, On reduced equations in the Hamiltonian theory of weakly nonlinear surface waves, J. Fluid Mech. 272 (1994) 1–20.

[32] F.P. Bretherton, Resonant interactions between waves. The case of discrete oscillations, J. Fluid Mech. 20 (1964) 457.

[33] M. Stiassnie, L. Shemer, On the interaction of four water waves, Wave Motion 41 (2005) 307–328.

[34] Alex D.D. Craik, Wave Interactions and Fluid Flows, Cambridge University Press, 1986.

[35] R. Stuhlmeier, M. Stiassnie, Nonlinear dispersion for ocean surface waves, J. Fluid Mech. 859 (2019) 49–58.

[36] M.S. Longuet-Higgins, O.M. Phillips, Phase velocity effects in tertiary wave interactions, J. Fluid Mech. 12 (03) (1962) 333–336.

[37] S. Liao, D. Xu, M. Stiassnie, On the steady-state nearly resonant waves, J. Fluid Mech. 794 (2016) 175–199.

[38] Ø. Kristiansen, D. Fructus, D. Clamond, J. Grue, Simulations of crescent water wave patterns on finite depth, Phys. Fluids 17 (6) (2005) 064101.

[39] D.I. Meiron, P.G. Saffman, H.C. Yuen, Calculation of steady three-dimensional deep-water waves, J. Fluid Mech. 124 (1982) 109–121.
[40] X. Yang, J. Yang, Z. Liu, On the steady-state exactly resonant, nearly resonant, and non-resonant waves and their relationships, Phys. Fluids 34 (8) (2022) 082107.
[41] A. Armaroli, D. Eeltink, M. Brunetti, J. Kasparian, Nonlinear stage of Benjamin-Feir instability in forced/damped deep-water waves, Phys. Fluids 30 (1) (2018) 1–9.
[42] A. Chabchoub, B. Kibler, J.M. Dudley, N. Akhmediev, Hydrodynamics of periodic breathers, Philos. Trans. R. Soc. A 372 (2027) (2014).
[43] G. Genty, A. Mussot, A. Chabchoub, J.M. Dudley, F. Dias, Rogue waves and analogies in optics and oceanography, Nat. Rev. Phys. 1 (2019) 675–689.
[44] G. Vanderhaegen, C. Naveau, P. Szriftgiser, A. Kudlinski, M. Conforti, A. Mussot, M. Onorato, S. Trillo, A. Chabchoub, N. Akhmediev, Extraordinary modulation instability in optics and hydrodynamics, Proc. Natl. Acad. Sci. 118 (14) (2021) e2019348118.